HHS Public Access

Author manuscript

Sci Immunol. Author manuscript; available in PMC 2020 June 06.

Published in final edited form as:

Sci Immunol. 2019 December 06; 4(42): . doi:10.1126/sciimmunol.aay8556.

T-cell-derived Interferon-γ programs stem cell death in immune-mediated intestinal damage

S. Takashima[1,§], **M. L. Martin**[2,§], **S. A. Jansen**[1,3,§], **Y. Fu**[1], **J. Bos**[3], **D. Chandra**[1], **M. H. O'Connor**[1], **A. M. Mertelsmann**[1], **P. Vinci**[1], **J. Kuttiyara**[1], **S. M. Devlin**[4], **S. Middendorp**[3], **M. Calafiore**[1], **A. Egorova**[1], **M. Kleppe**[1], **Y. Lo**[5], **N. F. Shroyer**[5], **E. H. Cheng**[6,7,8], **R. L. Levine**[1,6,9], **C. Liu**[10], **R. Kolesnick**[2,§], **C. A. Lindemans**[3,11,§], **A. M. Hanash**[1,9,§,*]

[1]Department of Medicine, Memorial Sloan Kettering Cancer Center, New York, New York 10065, USA [2]Department of Molecular Pharmacology, Memorial Sloan Kettering Cancer Center, New York, New York 10065, USA [3]Division of Pediatrics, Regenerative Medicine Center, University Medical Center Utrecht, Utrecht University, 3508 AB Utrecht, The Netherlands [4]Department of Biostatistics and Epidemiology, Memorial Sloan Kettering Cancer Center, New York, New York 10065, USA [5]Department of Medicine, Baylor College of Medicine, Houston, Texas 77030, USA [6]Human Oncology and Pathogenesis Program, Memorial Sloan Kettering Cancer Center, New York, New York 10065, USA [7]Department of Pathology, Memorial Sloan Kettering Cancer Center, New York, New York 10065, USA [8]Department of Pathology and Laboratory Medicine, Weill Cornell Medical College, Cornell University, New York, New York 10065, USA [9]Department of Medicine, Weill Cornell Medical College, New York, New York 10065, USA [10]Department of Pathology & Laboratory Medicine, Rutgers New Jersey Medical School, Newark, NJ 07103, USA [11]Princess Máxima Center for pediatric oncology, 3584 CS, Utrecht, The Netherlands

Abstract

Despite the importance of intestinal stem cells (ISCs) for epithelial maintenance and the significance of epithelial injury in immune-mediated intestinal diseases, there is limited understanding of how immune-mediated damage impacts ISCs and their niche. We found that stem cell compartment injury is a shared feature of both alloreactive and autoreactive intestinal immunopathology, reducing ISCs and impairing their recovery in T-cell-mediated injury models. While imaging revealed few T cells near the stem cell compartment in healthy mice, donor T cells infiltrating the intestinal mucosa after allogeneic bone marrow transplantation (BMT) primarily localized to the crypt region lamina propria. Further modeling with *ex vivo* epithelial cultures

*Correspondence to hanasha@mskcc.org.

§Contributed equally

Author contributions: S.T. designed, performed, and analyzed *in vivo* and *ex vivo* experiments and drafted the manuscript. M.L.M. designed, performed, and analyzed experiments including the mouse ISC colony assay. S.A.J. performed and analyzed *in vivo* experiments and human *ex vivo* experiments. J.B. performed and analyzed human *ex vivo* experiments. Y.F., J.K., D.C., M.H.O., A.M.M. and P.V. performed and analyzed *in vivo* experiments. S.M.D. assisted with statistical analyses. S.M. provided input and the human organoids and helped with various assays. M.C. provided input and helped with various assays. A.E. and J.K. performed and monitored bone marrow transplants and maintained the mouse colonies. M.K. and R.L.L. assisted with Jak1 deficiency experiments. Y.H.L. and N.F.S. assisted with Paneth cell deficiency experiments. E.H.C. provided input and helped with apoptosis assays. C.L. analyzed intestinal histopathology. R.K., C.A.L., and A.M.H. supervised the research.

Data and materials availability: The RNA sequencing data used in this study have been deposited in the GEO under the accession number GSE139813.

indicated ISC depletion and impaired human as well as murine organoid survival upon co-culture with activated T cells, and screening of effector pathways identified Interferon-γ as a principal mediator of ISC compartment damage. Interferon-γ induced JAK1- and STAT1-dependent toxicity, initiating a pro-apoptotic gene expression program and stem cell death. BMT with Interferon-γ-deficient donor T cells, with recipients lacking the Interferon-γ receptor (IFNγR) specifically in the intestinal epithelium, and with pharmacologic inhibition of JAK signaling all resulted in protection of the stem cell compartment. Additionally, epithelial cultures with Paneth-cell-deficient organoids, IFNγR-deficient Paneth cells, IFNγR-deficient ISCs, and purified stem cell colonies all indicated direct targeting of the ISCs that was not dependent on injury to the Paneth cell niche. Dysregulated T cell activation and Interferon-γ production are thus potent mediators of ISC injury, and blockade of JAK/STAT signaling within target tissue stem cells can prevent this T-cell-mediated pathology.

One Sentence Summary

T-cell-derived IFNγ can directly target intestinal stem cells to induce their apoptosis in a JAK/STAT-dependent manner.

Introduction

Epithelial stem cells are critical for physiologic self-renewal as well as regeneration after injury (1). The trans-membrane protein leucine-rich repeat-containing G protein-coupled receptor 5 (Lgr5) marks crypt base columnar intestinal stem cells (ISCs) capable of regenerating all the cells of the epithelium in the small intestine (SI) and large intestine (LI) (2). Paneth cells, which are progeny of ISCs, provide an epithelial niche for $Lgr5^+$ ISCs in SI by producing growth factors including Wnt3 and epidermal growth factor (EGF) (3, 4). Despite the importance of the stem cell compartment for epithelial maintenance and regeneration after gastrointestinal (GI) damage (5, 6), and despite increasing evidence for immunologic effects on tissue regeneration (7–9), there is little understanding of the effects of immune-mediated damage on tissue stem cells.

The GI tract is a frequent site of tissue damage after allogeneic hematopoietic/bone marrow transplantation (BMT), and injury to intestinal crypt epithelium is a characteristic finding of graft vs. host disease (GVHD) in transplant recipients (10, 11). GVHD is an immune-mediated complication of BMT in which donor T cells attack recipient tissues. The crypts contain the stem cells and progenitors of the intestinal epithelium, and it has been reported that both ISCs and their Paneth cell niche are reduced in mice with GVHD (8, 12–15). However, the mechanisms leading to their loss, the relationship between these cell populations during tissue injury, and the relevance of these findings to tissue damage beyond the transplant setting are all poorly understood.

Cytotoxicity and cytokine production are principal effector functions of T cells, and both functions have been studied considerably in GVHD models (16–29). Although T cells can mediate potent tissue damage in the GI tract, the impacts of cytokine signaling and cytotoxicity on the ISC compartment are not well defined. Inflammatory cytokines such as IFNγ and TNFα have been associated with damage to the Paneth cell niche (30–32), and

IFNγ contributes to reduced epithelial proliferation in mice with colitis (33). In contrast to how group 3 innate lymphoid cells and IL-22 can signal to ISCs to protect them and promote epithelial regeneration, it is possible that there are also direct interactions between ISCs and inflammatory cytokines during pathologic immune responses that compromise the ISC compartment. We thus sought to examine the specific cellular interactions and molecular mechanisms underlying ISC loss in immune-mediated GI damage. Using a combination of phenotypic and functional characterizations of the ISC compartment after alloreactive and autoreactive intestinal injury *in vivo*, coupled with *ex vivo* modeling of T cell interactions with ISCs and their Paneth cell niche in organoid cultures, we found that ISCs can be directly targeted by T-cell-derived cytotoxic cytokine signaling.

Results

Alloreactive and autoreactive immune responses impair the intestinal stem cell compartment

We first evaluated ISC kinetics in a clinically relevant major histocompatibility complex (MHC)-matched allogeneic BMT model. Three days after transplantation, BMT recipients receiving marrow alone (no GVHD) or marrow and T cells (for induction of GVHD) both demonstrated a reduction in SI $Lgr5^+$ ISCs compared to normal mice (Fig. 1, A and B, top panels). On day 10 post-BMT, $Lgr5^+$ ISC numbers had recovered in recipients transplanted without T cells, but ISC numbers remained reduced in GVHD recipients transplanted with donor T cells, demonstrating impairment of ISC recovery in immune-mediated GI damage occurring after BMT (Fig. 1, A and B, bottom panels). In contrast, $lysozyme^+$ Paneth cell numbers remained intact early after transplant, but were reduced by day 10 post-BMT in GVHD mice (Fig. 1C and fig. S1A), indicating that ISCs were reduced prior to Paneth cells after allogeneic BMT. Testing an independent haploidentical MHC-mismatched model also demonstrated rapid $Lgr5^+$ ISC reduction followed by substantial recovery in mice without GVHD, but persistent diminution of $Lgr5^+$ ISCs in T cell recipients (Fig. 1D). Once again, reduction of Paneth cells in this model only occurred following the reduction of ISCs (Fig. 1E and fig. S2).

To determine if these effects were specific to alloreactive damage and BMT, we examined the ISC compartment during systemic autoimmunity by crossing *Foxp3*-diphtheria toxin receptor (DTR) mice (34) with Lgr5-LacZ reporters. Mutations in the *FOXP3* gene in humans result in IPEX (Immune dysregulation, polyendocrinopathy, enteropathy, X-linked) syndrome, which is frequently associated with intestinal pathology (35), and ablation of $Foxp3^+$ regulatory T cells (Tregs) in mice leads to rapid systemic and intestinal autoimmune responses as well (36). Induction of systemic autoimmunity by DT-mediated Treg depletion quickly resulted in fewer $Lgr5^+$ ISCs, while Paneth cell numbers were maintained (Fig. 1, F and G). Reduction of ISCs was thus a shared feature of alloreactive and autoreactive immune-mediated GI damage, and it occurred prior to epithelial niche impairment as manifested by Paneth cell deficiency.

We next evaluated the effects of immune-mediated damage on the ISC compartment functionally, assessing *ex vivo* organoid-forming capacity after *in vivo* challenge. Intestinal crypts are functional units containing epithelial stem, progenitor, and niche cells, and

isolated crypts can generate intestinal organoids *ex vivo*. These organoids recapitulate *in vivo* intestinal organization with crypt-villus structures and central lumens (37). Consistent with the $Lgr5^+$ ISC frequencies (Fig. 1, A–B and D), SI crypts isolated early post-transplant demonstrated significant impairment in organoid-forming capacity compared to normal mice (Fig. 1H). The functional ability to generate organoids rapidly recovered in crypts from mice without GVHD, but organoid formation remained impaired ten days after BMT with allogeneic T cells (Fig. 1I). Likewise, in comparison to cultures from control mice, Treg depletion *in vivo* significantly impaired *ex vivo* organoid formation from isolated crypts (Fig. 1J). Furthermore, we also examined the *in vivo* function of ISCs after BMT using genetic marking of the stem cells and their progeny. In addition to Lgr5, Olfm4 also marks ISCs in mouse SI, and Olfm4-driven Cre expression has been shown to be more robust than that of Lgr5 (38). We thus performed allogeneic BMT into *Olfm4-CreERT2xRosa26* reporter mice, treating the BMT recipients with Tamoxifen prior to transplantation to activate Cre-driven lineage tracing (fig. S3). In comparison to normal controls, transplanted mice demonstrated reduced tracing from $Olfm4^+$ cells, even in the absence of donor T cells, suggesting ISC damage due to the pre-transplant conditioning. Moreover, BMT with T cells led to significant further reduction in tracing, providing additional functional validation for the loss of ISCs in GVHD (fig. S3). In total, both alloreactive and autoreactive *in vivo* immune responses resulted in reduction of ISCs and functional impairment of the stem cell compartment.

Allogeneic T cells preferentially invade crypt region lamina propria after BMT

In order to examine the intramucosal localization of T cells mediating epithelial injury and ISC reduction after BMT, we next performed 3-D confocal microscopy of intact whole-mount intestinal tissue. This approach has recently identified preferential infiltration of crypt region mucosa after allogeneic BMT (39), but such localization has not been distinguished between the intraepithelial and lamina propria components of the mucosa, and it has not been defined in homeostasis either. After staining for CD3, nuclei, and cellular membranes, imaging of full-thickness ileum allowed for accurate determination of mucosal architecture as well as precise localization and quantification of T cells in the epithelial and lamina propria regions of SI crypt and villus compartments. Normal B6 mice demonstrated similar T cell densities in crypt and in villus regions of ileal lamina propria at steady state (Fig. 2, A and B). In contrast, intraepithelial T cells were much more abundant in villus epithelium than in crypt epithelium at steady state (Fig. 2, A and B).

We next evaluated the location of donor T cells in recipient intestinal mucosa after allogeneic BMT, using B6-GFP mice as the source of donor T cells. Four days post-transplant, the early infiltration of GFP^+ donor T cells in recipient ileum was primarily located in the lamina propria of the crypt region, and few donor T cells could be identified in the villi (Fig. 2, C and D). Three days later, donor T cell invasion of the mucosa was much more substantial, and again most donor T cells were located in the crypt region lamina propria (Fig. 2, E and F). In contrast to intraepithelial T cells in B6 ileum at steady state, intraepithelial donor T cells one week after BMT were significantly more frequent in the crypts than in the villi (Fig. 2, E and F). These results indicated that donor T cells mediating GVHD primarily infiltrated the lamina propria of the crypt region, in proximity to the ISC

compartment, and most donor T cells invading the intestinal epithelium after BMT were present in the crypt region as well.

Activated T cells produce IFNγ that targets the intestinal epithelium, reduces ISCs, and eliminates organoids *ex vivo*

Investigation of T-cell-derived molecules mediating tissue injury can be complicated by redundancies in effector pathways and by the numerous potential targets that may exhibit divergent responses to similar molecules (16–29, 40, 41). Additionally, some conflicting experimental results may be due in part to the lack of models for studying specific interactions between immune effectors and primary cells as well as to challenges in deciphering responses against specific cellular subsets within a tissue. As such, we sought to establish a model for studying interactions between T cells and the ISC compartment by culturing intestinal organoids with T cells *ex vivo*. While co-culture with naive allogeneic T cells had no effect on regeneration from dissociated mouse organoid cells, allo-activated T cells significantly reduced allogeneic SI and LI organoid numbers in a concentration-dependent fashion (Fig. 3A and fig. S4A). Co-culture with polyclonally-activated allogeneic T cells also impaired organoid formation, and both $CD4^+$ and $CD8^+$ T cells were able to mediate organoid suppression (fig. S4, B and C). In addition to murine co-cultures, human T cells suppressed the growth of genetically disparate human duodenal organoids as well (Fig. 3B).

As organoid formation and survival were impaired by activated allogeneic T cells but not by naive allogeneic T cells (Fig. 3A), we hypothesized that antigenic disparity was important for T cell activation but was not required for target suppression once the T cells were already activated. Indeed, syngeneic co-cultures with allo-activated T cells or with polyclonally-stimulated T cells both impaired the viability of mouse organoids (Fig. 3C and fig. S4D). Furthermore, upon co-culturing T cells and organoids from the same donors, activated human $CD4^+$ and $CD8^+$ T cells suppressed the growth of autologous human colon organoids (Fig. 3D). These findings indicated that T cell activation can impair the viability of intestinal epithelium *ex vivo*, even in the absence of genetic disparity with the epithelial targets.

In order to define the T cell effector pathways mediating organoid toxicity, we performed co-cultures under several conditions with either genetically-deficient T cells or with neutralizing antibodies. Inhibition of perforin, FasL, TRAIL, IL-1β, IL-6, IL-17A, IL-22, and TNFα had no effect on organoid numbers (fig. S5, A to F). In contrast, T cell co-culture with anti-Interferon-γ (IFNγ) neutralizing antibodies restored murine SI organoid growth (Fig. 3E), and IFNγ blockade with neutralizing antibodies also protected human duodenal organoids from human allogeneic T cells (Fig. 3F). Anti-IFNγ antibodies could have protected organoids by preventing paracrine/autocrine IFNγ activity among the T cells or by suppressing IFNγ signaling within the organoids. However, *Ifngr*$^{-/-}$ T cells demonstrated intact organoid suppression (fig. S5, G and H), while *Ifngr*$^{-/-}$ organoids were significantly resistant to both allogeneic and syngeneic T cells (Fig. 3G and fig. S5I), indicating that IFNγ targeted the epithelium during co-culture.

IFNγ alone was sufficient for mediating organoid toxicity, as addition of recombinant murine (rm) IFNγ to cultures without T cells demonstrated concentration-dependent

suppression of organoid numbers (Fig. 3H). Tracking T cell kinetics in co-cultures using GFP^+ T cells, we found that T cell frequencies decreased by day 4 of the culture (Fig. 3I and fig. S4E), suggesting that IFNγ-mediated organoid suppression was initiated within the first few days of the culture. Consistent with this, IFNγ was detected in the culture media on day three of co-culture, and the concentration decreased by day five (Fig. 3J). Moreover, flow cytometry analysis showed a significant reduction of Lgr5-GFP^{high} ISCs in organoids after 16 hours of incubation with IFNγ, and this ISC depletion progressed substantially by 72 hours after exposure to IFNγ (Fig. 3K).

IFNγ programs stem cell death, and Inhibition of JAK/STAT signaling protects ISCs from IFNγ

We next investigated the signaling pathways involved in IFNγ-mediated organoid and ISC suppression. Ruxolitinib is a JAK 1/2 inhibitor capable of preventing T cell function, suppressing production of inflammatory cytokines by $CD4^+$ T cells and promoting increased frequencies of $Foxp3^+$ regulatory T cells in the BMT setting (42). Recent work has established ruxolitinib as a therapeutic option in GVHD, particularly for steroid refractory disease, and it has received FDA approval for this indication (43–45). However, the potentially distinct effects of ruxolitinib on T cells and on target tissues have yet to be delineated. We found that ruxolitinib significantly protected intestinal organoids from allogeneic T cells *ex vivo* (Fig. 4A). Ruxolitinib also protected mouse (Fig. 4B) and human (Fig. 4C) intestinal organoids from IFNγ. Furthermore, ISC frequencies were significantly preserved in organoids cultured with IFNγ in the presence of ruxolitinib, including near-total preservation in the first 16 hours and partial preservation by 72 hours (Fig. 4D).

Protection of organoids from IFNγ in the absence of T cells suggested that ruxolitinib was acting on the organoids themselves, mediating resistance by suppressing epithelial JAK signaling. Using organoids from *Jak1*-floxed x Rosa-cre-ert2 mice, we found that passaged organoid cells pretreated with 4-OHT to delete Jak1 were resistant to allogeneic T cells and to IFNγ (Fig. 4E and fig. S6). Furthermore, ruxolitinib prevented phosphorylation of Stat1 by IFNγ in SI crypts (Fig. 4F), and $Stat1^{-/-}$ organoids were resistant to IFNγ as well (Fig. 4G). We thus concluded that allogeneic T cells and IFNγ targeted the intestinal epithelium via Jak1/STAT1 signaling, and inhibition of epithelial Jak1 could protect intestinal tissue from immune-mediated damage *ex vivo*.

In addition to the reduction of ISCs identified by flow cytometry (Fig. 3K), qPCR analysis of intestinal organoids showed that gene expression associated with ISCs (*Lgr5, Olfm4*) decreased quickly in mouse and human cultures treated with IFNγ (fig. S7, A and B). Target genes of Wnt signaling (*Axin2*) and Notch signaling (*Hes1*) were also reduced (fig. S7C), and gene expression associated with Paneth cells (*Lyz1, Defa1*), enterocytes (*Alpi*), goblet cells (*Muc2*), enteroendocrine cells (*Chga*), and tuft cells (*Trpm5*) were all reduced as well (Fig. S7, D and E). Consistent with these results, qPCR analysis of crypts from GVHD recipients demonstrated reduced gene expression associated with ISCs (*Lgr5*, *Olfm4*), Paneth cells (*Lyz1*, *Defa1*), goblet cells (*Muc2*), enteroendocrine cells (*Chga*), and tuft cells (*Trpm5*) in comparison with non-GVHD controls, while enterocyte-associated *Alpi* expression trended down even after BMT without T cells (fig. S7F). Overall, these gene

expression patterns suggested that ISCs were not being lost due to increased differentiation of ISCs into their progeny.

We next evaluated the role of programmed cell death. Gene expression in mouse SI organoids cultured with IFNγ demonstrated multiple transcriptional changes consistent with induction of apoptosis, as expression of the anti-apoptotic genes *Bcl2 and Bcl2l1* (*Bcl-x_L*) decreased and expression of the pro-apoptotic gene *Bak* increased (Fig. 5A). Similar transcriptional changes were observed in human duodenal organoids treated with IFNγ (Fig. 5B). No changes were observed in expression of the anti-apoptotic gene *Mcl1* or the pro-apoptotic gene *Bax* (fig. S8A). Moreover, Annexin V analysis showed increased Annexin $^{+}$DAPI^{-} and Annexin^{+}DAPI^{+} Lgr5-GFP^{+} cells after IFNγ treatment, consistent with increased early apoptotic and dead ISCs, even though there was already a statistically significant reduction in ISC frequency at that point (Fig. 5, C and D). Increased apoptosis was also identified in human intestinal organoids incubated with IFNγ, as determined by increased caspase-3/7 activity and confirmed by increased detection of cleaved caspase-3 (Fig. 5, E and F). Additionally, ruxolitinib inhibited the pro-apoptotic transcriptional changes observed in intestinal organoids treated with IFNγ (Fig. 5G), thus specifically linking JAK signaling to the apoptotic phenotype. Therefore in total, *ex vivo* experiments indicated that T cells induced organoid toxicity via IFNγ, which activated JAK1-dependent STAT1 activation within the epithelium, resulting in an apoptotic transcriptional program and loss of ISCs.

T-cell-derived IFNγ promotes stem cell apoptosis and intestinal pathology in immune-mediated GI damage *in vivo*

We next sought to evaluate the role of IFNγ in T-cell-mediated stem cell injury *in vivo*. Anti-IFNγ antibody treatment after allogeneic BMT significantly protected ISC numbers in Lgr5-LacZ reporter mice (Fig. 6A). Additionally, anti-IFNγ neutralizing antibodies increased ISC frequencies during autoimmunity occurring after Treg depletion (Fig. 6B). Furthermore, ruxolitinib treatment significantly protected ISCs in transplant recipients after allogeneic BMT (Fig. 6C and fig. S1B).

To identify *in vivo* sources of IFNγ promoting ISC reduction post-BMT, we first phenotyped IFNγ^{+} cells in the mucosa of transplant recipients. After mechanically dissociating the villi to enrich for crypt region tissue, lamina propria lymphocytes (LPLs) were isolated and incubated with a golgi inhibitor prior to IFNγ analysis. Substantially more IFNγ^{+} cells were identified in recipient intestinal mucosa after allogeneic BMT than after syngeneic BMT, and the vast majority of the IFNγ^{+} cells identified were indeed donor T cells (fig. S9, A and B). Further analysis indicated T-bet^{+} Th1 helper T cells with an activated phenotype (fig. S9, C and D).

We next evaluated donor-derived IFNγ functionally. While transplantation with *Ifng*$^{-/-}$ donor marrow did not impact ISC numbers (Fig. 6D), allogeneic BMT with *Ifng*$^{-/-}$ donor T cells resulted in significantly greater ISC recovery (Fig. 6E), confirming donor T cells to be the critical source of IFNγ resulting in ISC reduction. Furthermore, broader histopathologic analysis after BMT with *Ifng*$^{-/-}$ donor T cells showed significant reduction in overall GVHD pathology, including reduced SI crypt loss and villus blunting (Fig. 6, F and G, and

fig. S1C). In addition, we observed increased epithelial proliferation along with the tissue injury occurring in GVHD, which was also significantly reduced in recipients of IFNγ-deficient T cells (Fig. 6H).

Similar to the gene expression changes induced by IFNγ *ex vivo*, qPCR analysis of crypts isolated post-BMT indicated increased *Bcl2,* increased *Bcl2l1,* and decreased *Bak1* in recipients of *Ifng*$^{-/-}$ T cells (Fig. 6I). Additionally, anti-cleaved-caspase-3 and TUNEL staining both indicated significantly reduced crypt apoptosis in mice transplanted with *Ifng*$^{-/-}$ T cells (Fig. 6, J to L). Furthermore, anti-cleaved-caspase-3 and anti-β-gal double immunofluorescent staining demonstrated apoptotic Lgr5^{+} ISCs in GVHD, and the frequency of cleaved caspase-3^{+} ISCs was significantly reduced in mice receiving *Ifng*$^{-/-}$ T cells (Fig. 6L and fig. S10). Finally, SI crypts isolated from recipients of *Ifng*$^{-/-}$ T cells demonstrated significantly greater organoid formation than crypts from mice transplanted with wild-type (WT) T cells (Fig. 6M), indicating functional improvement in addition to the improved histology. Overall, *in vivo* studies thus supported the *ex vivo* findings of ISC reduction induced by T-cell-derived IFNγ and JAK/STAT signaling.

IFNγ directly targets intestinal stem cells and induces apoptosis

Given the broad expression of the IFNγ receptor (IFNγR) on numerous cell types, T-cell-derived IFNγ could have many targets *in vivo*, leading to indirect effects on the stem cell compartment. To examine if T-cell-derived IFNγ was targeting the recipient epithelium directly *in vivo*, we performed allogeneic BMT into *Ifngr1*$^{fl/fl}$ x Villin-Cre (*Ifngr*$^{\Delta IEC}$) mice. Staining for Olfm4 indicated that targeted deletion of IFNγR from recipient intestinal epithelium significantly protected Olfm4^{+} ISCs from allogeneic T cells (Fig. 7A and fig. S1D). *Ifngr*$^{\Delta IEC}$ recipients also demonstrated reduced overall GVHD pathology, greater crypt numbers, decreased villus blunting, and significantly less crypt apoptosis (Fig. 7, B to D).

These results indicated that IFNγ could act directly on the intestinal epithelium, but it remained possible that effects on ISCs were secondary to targeting some other cell population in the intestinal epithelium. Crypt base ISCs repopulate other intestinal epithelial cells including Paneth cells, which produce several supportive factors such as Wnt3, EGF, and Notch ligands (4). As Paneth cell frequencies and gene expression were reduced in our experiments (Fig. 1, C and E, fig. S2B, and fig. S7, D and F), and IFNγ can induce apoptosis and loss of Paneth cells (30, 31), ISC reduction and organoid elimination could have been due to indirect effects resulting from damage to the Paneth cell niche. FACS analysis confirmed expression of IFNγR1 (CD119) on both Paneth cells and ISCs (Fig. 7E and fig. S2A). Given that ISC-restricted cre-driven gene deletion is not possible *in vivo* because genetic manipulation of ISCs is rapidly transmitted to their progeny (with faster kinetics than GVHD pathophysiology and at times even faster kinetics than the genetic manipulation can manifest protein-level changes within the ISCs), we therefore examined *ex vivo* if T-cell-mediated injury was due to targeting of the ISCs or Paneth cells. Arguing against an essential role for Paneth cell targeting, supplementation of the culture media with the Paneth-cell-derived factors Wnt3 and Jagged1 did not protect intestinal organoids from T cells (Fig. 7F). Similarly, prevention of Paneth cell targeting through use of Paneth-cell-

deficient *Atoh1*$^{\Delta IEC}$ organoids did not protect the organoids from T cells or IFNγ either (Fig. 7G). We next co-cultured purified ISCs and purified Paneth cells such that organoid formation from ISCs was dependent on support provided by the Paneth cells. However, cultures with WT and *Ifngr*$^{-/-}$ Paneth cells both remained sensitive to T cells (Fig. 7H). Additionally, RNA sequencing of sorted Lgr5^{high} cells 1.5 hours after exposure to IFNγ showed upregulation of several IFNγ-related genes confirming direct activity of IFNγ in ISCs (Fig. 7I). Moreover, organoid growth from WT ISCs was significantly reduced by co-culture with allogeneic T cells, but *Ifngr*$^{-/-}$ ISCs demonstrated intact organoid-forming capacity and were thus resistant to T-cell-mediated suppression (Fig. 7J).

To exclude the possibility that cultures of WT ISCs were sensitive to IFNγ because of damage to their immediate progeny and to further evaluate the direct effects of IFNγ on ISCs, we utilized a niche-independent high-purity ISC culture system composed nearly entirely of Lgr5^{+} cells (46). Combination of GSK3β and histone deacetylase inhibitors enables culture of homogenous symmetrically dividing Lgr5^{+} ISC colonies from purified ISCs, and despite the potent Wnt and Notch pathway activation maintaining a high Lgr5^{+} frequency (fig. S8B), IFNγ directly induced apoptosis within the ISC colonies (Fig. 7K). As evidenced by staining for cleaved caspase-3, apoptotic ISCs identified within the cellular layer of the colonies peaked after eight hours (Fig. 7, K and L) and subsequently accumulated in the colony lumen (Fig. 7, K and M). Gene expression analyses revealed the same apoptotic program identified in organoids exposed to IFNγ, with downregulation of *Bcl2* and *Bcl2l1,* upregulation of *Bak*, and no significant change in expression of *Mcl1* or *Bax* (Fig. 7N and fig. S8C). IFNγ-induced ISC apoptosis also led to substantial colony death confirmed by propidium iodide uptake (Fig. 7, O and P). Furthermore, addition of the pan-caspase inhibitor Q-VD-Oph to WT ISC colonies (Fig. 7, O and Q) or genetic deletion of *Bak* and *Bax* using ISC colonies derived from double-deficient (*Bak*$^{-/-}$/*Bax*-floxed x Rosa-cre-ert2) mice (Fig. 7, P and Q) both maintained ISC colony viability despite exposure to IFNγ. In conclusion, T-cell-derived IFNγ directly targeted the intestinal epithelium leading to ISC reduction and intestinal pathology, and IFNγ induced Bak/Bax-dependent ISC apoptosis by directly acting on the stem cells themselves.

Discussion

T-cell-mediated tissue damage, particularly in the BMT setting, is the culmination of a systemic process involving cellular activation, migration, and effector function. Given this complexity and the involvement of numerous cell types in various tissues at specific time points, it is challenging to comprehensively and accurately elucidate the specific interactions occurring between T cells and individual subsets of intestinal epithelial cells. To overcome these limitations, we established an *ex vivo* co–culture system of intestinal organoids and T cells. Using this system to model T-cell-induced ISC damage, we identified a direct role for T-cell-derived IFNγ and subsequent JAK/STAT signaling in ISC apoptosis occurring during immune-mediated GI damage. Consistent with this cytokine-mediated pathology, whole-mount 3-D microscopy after allogeneic BMT demonstrated that donor T cells invading the SI post-transplant primarily infiltrated the lamina propria of the crypt compartment. Donor T cells thus invaded the intestinal mucosa near the stem cells, but were mostly not located precisely within the targeted epithelium. Further analysis of these T cells confirmed that they

were the principle source of IFNγ. Surprisingly, few T cells were present within the crypt epithelium at baseline, as most intraepithelial T cells were found within the villi. The lamina propria showed roughly similar T cell densities within the crypt and villus regions at baseline, so the preferential infiltration of the crypt region after allogeneic BMT represented a substantial redistribution of T cell localization within the mucosa of the ileum. Interestingly, a recent study showed that depletion of donor $CD4^+$ T cells immediately after BMT resulted in increased serum IFNγ and reduced intestinal GVHD pathology with fewer donor $CD8^+$ T cells in the colon (47), suggesting that IFNγ from donor T cells in proximity to the crypt compartment, rather than the IFNγ present in circulation, may be essential for its direct epithelial toxicity.

While naive T cells had no impact on epithelial growth in *ex vivo* cultures, activated T cells induced substantial toxicity and reduction of ISCs. This did not require genetic disparity between the T cells and their epithelial targets once the T cells were activated, leading to suppression of both allogeneic and syngeneic mouse intestinal organoids. This was also true in human models, with human T cells eliminating allogeneic human organoids and even eliminating autologous organoids as well. This was driven by T-cell-derived IFNγ, which also induced the ISC reduction observed *ex vivo* as well as *in vivo*. Antigen specificity in this *ex vivo* model was dependent on the initial T cell activation, which led to substantial production of IFNγ. These results are consistent with experiments indicating that inflammatory cytokines can mediate tissue damage induced by allogeneic T cells irrespective of antigen presentation by epithelial cells (48), although antigen presentation by epithelial cells including ISCs may be critical for certain other immune responses (49–51).

Effects of IFNγ on the GI tract have been studied in various experimental models, and it has been reported to induce epithelial toxicity through both cell-autonomous and non-autonomous negative regulatory feedback loops (33, 52, 53). IFNγ has also been found to induce loss of Paneth cells in models of infection and autoimmunity (30, 31). Studies in transplant models have identified both pathologic and protective roles for IFNγ in GVHD, as discussed below. However, there has been little exploration of the direct interactions between ISCs and IFNγ. The exclusive use here of primary cells, containing the full diversity of lineages present in normal epithelial tissue, allowed for identification of ISCs as direct targets of T-cell-mediated cytokine-dependent GI damage. This would not have been possible with typical cell lines lacking a stem cell compartment. We found that reduction of ISCs preceded any reduction of Paneth cells in immune-mediated GI damage. The reduction of ISCs was validated using two distinct functional approaches: culturing organoids from crypts isolated after *in vivo* challenge and lineage tracing for stem cell-derived progeny. Both functional approaches were consistent with the kinetics indicated by ISC quantifications. Furthermore, these kinetics suggested that ISCs were the primary target, though a decrease in ISCs could also have been due to niche dysfunction, rather than loss of the niche. While Paneth cells are not the only component of the stem cell niche, which includes stromal and immunologic members as well (8, 9, 14, 54, 55), and consideration should also be paid to progenitors and mature epithelial cells for a comprehensive understanding of intestinal immunopathology (56–59), *ex vivo* modeling revealed that IFNγ-receptor-deficient ISCs were resistant to T cells and IFNγ, while niche-dependent cultures of ISCs with IFNγ-receptor-deficient Paneth cells as well as cultures of niche-

independent stem cell colonies were not. These findings thus indicated that ISCs were indeed direct targets of T cells and IFNγ.

Further investigation of the stem cell compartment indicated that IFNγ could directly program ISC death. BCL-2 and BCL-X_L are anti-apoptotic BCL-2 family members, and their downregulation can result in activation of pro-apoptotic effectors BAX and BAK (60). Activated BAX and BAK can then form oligomers which permeabilize the mitochondrial outer membrane and release cytochrome c to activate caspases and further propagate the apoptotic cascade (61). The downregulation of *Bcl2* and *Bcl2l1*, and the upregulation of *Bak*, along with stable expression of *Bax* clearly implicate initiation of apoptosis as a major direct effect of IFNγ in ISCs. Furthermore, we observed increased caspase-3 activity and cleaved caspase-3 protein in human organoids treated with IFNγ. *In vivo* IFNγ signaling blockade with neutralizing antibodies, IFNγ deletion from donor T cells, IFNγR deletion from the intestinal epithelium, and ruxolitinib all protected ISCs from T cells *in vivo*. While the specific roles of IFNγ may be distinct between models of GVHD and autoimmunity, these results suggest that IFNγ is a potent mediator of T-cell-induced ISC impairment and that a secreted cytokine can kill stem cells via activation of JAK/STAT signaling and driving programmed cell death.

Due to its pleiotropic effects, IFNγ has demonstrated strikingly distinct impacts in various BMT models. Deficiency of donor-derived IFNγ resulted in increased GVHD mortality and limited GVL in a $CD8^+$ T-cell-mediated experimental transplant model (28). A subsequent study showed opposing effects of IFNγ in distinct tissues, with IFNγ playing a protective role in the lungs, but mediating GI toxicity in mice with GVHD (18), and another study indicated that IFNγ can reduce intestinal GVHD pathology after depletion of $CD4^+$ T cells (47). These studies illustrate the complex role of IFNγ after BMT, and undesirable complications could thus result from targeting IFNγ in clinical BMT. IFNγ signaling is transduced by the JAK/STAT pathway (62), which could represent another approach for interfering with IFNγ-mediated GI damage and loss of ISCs. Indeed, ruxolitinib treatment protected ISCs from T-cell-mediated damage *ex vivo* and *in vivo*. While JAK inhibition can suppress T cell activity (42), we found that it also protected intestinal epithelium from T-cell-mediated injury by suppressing the tissue's response to the T cells. JAK inhibition has been investigated clinically in GVHD (43–45), and it has recently been approved for steroid refractory GVHD. JAK inhibitors thus provide a promising approach for protecting the ISC compartment from pathologic immune responses. Additionally, these findings suggest that the efficacy of JAK inhibition in GVHD, particularly in settings where other immunosuppressive agents have failed, could be due to suppression of pathologic cytokine signaling within the GVHD target organs.

In summary, we found that damage to the ISC compartment was a shared feature of GVHD and autoimmunity, and T-cell-derived IFNγ was a key mediator of ISC reduction in immune-mediated GI damage. Intestinal organoid cultures were used to assay epithelial function during immune-mediated damage *in vivo* and to interrogate specific interactions between T cells and epithelial targets *ex vivo*. T cell localization within the intestinal mucosa differed substantially between homeostasis and the post-transplant setting, with donor T cells primarily localizing to the lamina propria of the crypt region where they were

the dominant producers of IFNγ. IFNγ directly targeted ISCs, inducing a gene expression program resulting in stem cell apoptosis, and JAK inhibition protected ISCs from T cells by suppressing their response to IFNγ. IFNγ thus played a central role in the T-cell-mediated stem cell damage, and JAK inhibitors may provide clinically efficacious immunosuppression in part by suppressing tissue responses to pathologic signals from the immune system.

Materials and Methods

Study design

The purpose of the study was to investigate mechanisms of T cell effects on ISCs during immune-mediated GI damage. We used two types of *in vivo* animal models: allogeneic BMT and Treg-depletion-induced autoimmunity. To perform detailed evaluation of direct interactions between T cells and ISCs, we established a method of co-culturing T cells with intestinal organoids. Analyses of experiments were performed with histologic staining, 3-D imaging, flow cytometry, qPCR, and western blotting. Statistical issues are described below. There were no pre-defined study end points. Experiments were generally performed a minimum of two times, and statistical methods are described in the figure legends.

For further details, please see the Supplementary Materials and Methods.

Supplementary Material

Refer to Web version on PubMed Central for supplementary material.

Acknowledgments

We thank Hans Clevers, Johan van Es, and Alexander Rudensky for generous sharing of mice and advice, and we gratefully acknowledge the technical assistance of the MSKCC Research Animal Resource Center and Molecular Cytology Core Facility. We thank Jarrod A. Dudakov, Enrico Velardi, Marcel R.M. van den Brink, Matthias Schewe, Riccardo Fodde, Jorik M. van Rijn and Edward E.S. Nieuwenhuis for their valuable advice. We also thank the Integrated Genomics Operation Core, funded by the NCI Cancer Center Support Grant (CCSG, P30 CA08748), Cycle for Survival, and the Marie-Josée and Henry R. Kravis Center for Molecular Oncology.

Funding: This research was supported by National Institutes of Health award numbers K08-HL115355 (A.M.H.), R01-HL125571 (A.M.H), R01-HL146338 (A.M.H), R01 CA125562 (E.C.), P01-CA108671 (R.L.L.), and P30-CA008748 (MSKCC Core Grant). Support was also received from the Susan and Peter Solomon Divisional Genomics Program, the Ludwig Center for Cancer Immunotherapy, the Parker Institute for Cancer Immunotherapy, the Anna Fuller Fund. and the Amy Strelzer Manasevit Research Program (A.M.H.). S.T. was supported by a scholarship from the Mochida Memorial Foundation for Medical and Pharmaceutical Research and an ASBMT (now ASTCT) New Investigator Award. Y.F. was also supported by an ASBMT/ASTCT New Investigator Award, and P.V. was supported by an ASBMT/ASTCT New Investigator Award and the American Italian Cancer Foundation. C.A.L. was supported by the WKZ fund of the UMC Utrecht, and S.A.J. was supported by the Jo Kolk Study Fund Foundation, Nijbakker-Morra Foundation, Dutch Digestive Foundation, K.F. Hein Foundation, Renswoude Foundation and Alexandre Suerman Stipend of the UMC Utrecht.

Competing interests: A.M.H. holds intellectual property related to Interleukin-22 and in the last three years has performed consulting for Ziopharm and Nexus Global Group. R.L.L. is on the supervisory board of Qiagen and is a scientific advisor to Loxo, Imago, C4 Therapeutics and Isoplexis, which include equity interest. He receives research support from and consulted for Celgene and Roche and has consulted for Lilly, Janssen, Astellas, Morphosys and Novartis. He has received honoraria from Roche, Lilly and Amgen for invited lectures and from Gilead for grant reviews. R.K. is a co-founder of Ceramedix Holding L.L.C., and holds the following patents: US10413533B2, US7195775B1, US7850984B2, US10052387B2, US8562993B2, US9592238B2, US20150216971A1, US20170335014A1, US20170333413A1, and US20180015183A1.

References and Notes

1. Gehart H, Clevers H, Repairing organs: lessons from intestine and liver. Trends Genet 31, 344–351 (2015). [PubMed: 25989898]
2. Barker N, van Es JH, Kuipers J, Kujala P, van den Born M, Cozijnsen M, Haegebarth A, Korving J, Begthel H, Peters PJ, Clevers H, Identification of stem cells in small intestine and colon by marker gene Lgr5. Nature 449, 1003–1007 (2007). [PubMed: 17934449]
3. Clevers H, The intestinal crypt, a prototype stem cell compartment. Cell 154, 274–284 (2013). [PubMed: 23870119]
4. Sato T, van Es JH, Snippert HJ, Stange DE, Vries RG, van den Born M, Barker N, Shroyer NF, van de Wetering M, Clevers H, Paneth cells constitute the niche for Lgr5 stem cells in intestinal crypts. Nature 469, 415–418 (2011). [PubMed: 21113151]
5. Barker N, Huch M, Kujala P, van de Wetering M, Snippert HJ, van Es JH, Sato T, Stange DE, Begthel H, van den Born M, Danenberg E, van den Brink S, Korving J, Abo A, Peters PJ, Wright N, Poulsom R, Clevers H, Lgr5(+ve) stem cells drive self-renewal in the stomach and build long-lived gastric units in vitro. Cell Stem Cell 6, 25–36 (2010). [PubMed: 20085740]
6. Metcalfe C, Kljavin NM, Ybarra R, de Sauvage FJ, Lgr5+ stem cells are indispensable for radiation-induced intestinal regeneration. Cell Stem Cell 14, 149–159 (2014). [PubMed: 24332836]
7. Taniguchi K, Wu LW, Grivennikov SI, de Jong PR, Lian I, Yu FX, Wang K, Ho SB, Boland BS, Chang JT, Sandborn WJ, Hardiman G, Raz E, Maehara Y, Yoshimura A, Zucman-Rossi J, Guan KL, Karin M, A gp130-Src-YAP module links inflammation to epithelial regeneration. Nature 519, 57–62 (2015). [PubMed: 25731159]
8. Lindemans CA, Calafiore M, Mertelsmann AM, O'Connor MH, Dudakov JA, Jenq RR, Velardi E, Young LF, Smith OM, Lawrence G, Ivanov JA, Fu YY, Takashima S, Hua G, Martin ML, O'Rourke KP, Lo YH, Mokry M, Romera-Hernandez M, Cupedo T, Dow LE, Nieuwenhuis EE, Shroyer NF, Liu C, Kolesnick R, van den Brink MR, Hanash AM, Interleukin-22 promotes intestinal-stem-cell-mediated epithelial regeneration. Nature 528, 560–564 (2015). [PubMed: 26649819]
9. Aparicio-Domingo P, Romera-Hernandez M, Karrich JJ, Cornelissen F, Papazian N, Lindenbergh-Kortleve DJ, Butler JA, Boon L, Coles MC, Samsom JN, Cupedo T, Type 3 innate lymphoid cells maintain intestinal epithelial stem cells after tissue damage. J Exp Med 212, 1783–1791 (2015). [PubMed: 26392223]
10. Epstein RJ, McDonald GB, Sale GE, Shulman HM, Thomas ED, The diagnostic accuracy of the rectal biopsy in acute graft-versus-host disease: a prospective study of thirteen patients. Gastroenterology 78, 764–771 (1980). [PubMed: 6986319]
11. Sale GE, Shulman HM, McDonald GB, Thomas ED, Gastrointestinal graft-versus-host disease in man. A clinicopathologic study of the rectal biopsy. Am J Surg Pathol 3, 291–299 (1979). [PubMed: 44107]
12. Eriguchi Y, Uryu H, Nakamura K, Shimoji S, Takashima S, Iwasaki H, Miyamoto T, Shimono N, Hashimoto D, Akashi K, Ayabe T, Teshima T, Reciprocal expression of enteric antimicrobial proteins in intestinal graft-versus-host disease. Biol Blood Marrow Transplant 19, 1525–1529 (2013). [PubMed: 23927965]
13. Jenq RR, Ubeda C, Taur Y, Menezes CC, Khanin R, Dudakov JA, Liu C, West ML, Singer NV, Equinda MJ, Gobourne A, Lipuma L, Young LF, Smith OM, Ghosh A, Hanash AM, Goldberg JD, Aoyama K, Blazar BR, Pamer EG, van den Brink MR, Regulation of intestinal inflammation by microbiota following allogeneic bone marrow transplantation. J Exp Med 209, 903–911 (2012). [PubMed: 22547653]
14. Hanash AM, Dudakov JA, Hua G, O'Connor MH, Young LF, Singer NV, West ML, Jenq RR, Holland AM, Kappel LW, Ghosh A, Tsai JJ, Rao UK, Yim NL, Smith OM, Velardi E, Hawryluk EB, Murphy GF, Liu C, Fouser LA, Kolesnick R, Blazar BR, van den Brink MR, Interleukin-22 protects intestinal stem cells from immune-mediated tissue damage and regulates sensitivity to graft versus host disease. Immunity 37, 339–350 (2012). [PubMed: 22921121]
15. Takashima S, Kadowaki M, Aoyama K, Koyama M, Oshima T, Tomizuka K, Akashi K, Teshima T, The Wnt agonist R-spondin1 regulates systemic graft-versus-host disease by protecting intestinal stem cells. J Exp Med 208, 285–294 (2011). [PubMed: 21282378]

16. Baker MB, Altman NH, Podack ER, Levy RB, The role of cell-mediated cytotoxicity in acute GVHD after MHC-matched allogeneic bone marrow transplantation in mice. J Exp Med 183, 2645–2656 (1996). [PubMed: 8676085]

17. Braun MY, Lowin B, French L, Acha-Orbea H, Tschopp J, Cytotoxic T cells deficient in both functional fas ligand and perforin show residual cytolytic activity yet lose their capacity to induce lethal acute graft-versus-host disease. J Exp Med 183, 657–661 (1996). [PubMed: 8627178]

18. Burman AC, Banovic T, Kuns RD, Clouston AD, Stanley AC, Morris ES, Rowe V, Bofinger H, Skoczylas R, Raffelt N, Fahy O, McColl SR, Engwerda CR, McDonald KP, Hill GR, IFNgamma differentially controls the development of idiopathic pneumonia syndrome and GVHD of the gastrointestinal tract. Blood 110, 1064–1072 (2007). [PubMed: 17449800]

19. Ellison CA, Fischer JM, HayGlass KT, Gartner JG, Murine graft-versus-host disease in an F1-hybrid model using IFN-gamma gene knockout donors. J Immunol 161, 631–640 (1998). [PubMed: 9670937]

20. Graubert TA, DiPersio JF, Russell JH, Ley TJ, Perforin/granzyme-dependent and independent mechanisms are both important for the development of graft-versus-host disease after murine bone marrow transplantation. J Clin Invest 100, 904–911 (1997). [PubMed: 9259590]

21. Jiang Z, Podack E, Levy RB, Major histocompatibility complex-mismatched allogeneic bone marrow transplantation using perforin and/or Fas ligand double-defective CD4(+) donor T cells: involvement of cytotoxic function by donor lymphocytes prior to graft-versus-host disease pathogenesis. Blood 98, 390–397 (2001). [PubMed: 11435308]

22. Murphy WJ, Welniak LA, Taub DD, Wiltrout RH, Taylor PA, Vallera DA, Kopf M, Young H, Longo DL, Blazar BR, Differential effects of the absence of interferon-gamma and IL-4 in acute graft-versus-host disease after allogeneic bone marrow transplantation in mice. J Clin Invest 102, 1742–1748 (1998). [PubMed: 9802888]

23. Na IK, Lu SX, Yim NL, Goldberg GL, Tsai J, Rao U, Smith OM, King CG, Suh D, Hirschhorn-Cymerman D, Palomba L, Penack O, Holland AM, Jenq RR, Ghosh A, Tran H, Merghoub T, Liu C, Sempowski GD, Ventevogel M, Beauchemin N, van den Brink MR, The cytolytic molecules Fas ligand and TRAIL are required for murine thymic graft-versus-host disease. J Clin Invest 120, 343–356 (2010). [PubMed: 19955659]

24. Robb RJ, Hill GR, The interferon-dependent orchestration of innate and adaptive immunity after transplantation. Blood 119, 5351–5358 (2012). [PubMed: 22517908]

25. Schmaltz C, Alpdogan O, Kappel BJ, Muriglan SJ, Rotolo JA, Ongchin J, Willis LM, Greenberg AS, Eng JM, Crawford JM, Murphy GF, Yagita H, Walczak H, Peschon JJ, van den Brink MR, T cells require TRAIL for optimal graft-versus-tumor activity. Nat Med 8, 1433–1437 (2002). [PubMed: 12426560]

26. Wang H, Asavaroengchai W, Yeap BY, Wang MG, Wang S, Sykes M, Yang YG, Paradoxical effects of IFN-gamma in graft-versus-host disease reflect promotion of lymphohematopoietic graft-versus-host reactions and inhibition of epithelial tissue injury. Blood 113, 3612–3619 (2009). [PubMed: 19211507]

27. Yang YG, Dey BR, Sergio JJ, Pearson DA, Sykes M, Donor-derived interferon gamma is required for inhibition of acute graft-versus-host disease by interleukin 12. J Clin Invest 102, 2126–2135 (1998). [PubMed: 9854048]

28. Yang YG, Qi J, Wang MG, Sykes M, Donor-derived interferon gamma separates graft-versus-leukemia effects and graft-versus-host disease induced by donor CD8 T cells. Blood 99, 4207–4215 (2002). [PubMed: 12010827]

29. Yi T, Chen Y, Wang L, Du G, Huang D, Zhao D, Johnston H, Young J, Todorov I, Umetsu DT, Chen L, Iwakura Y, Kandeel F, Forman S, Zeng D, Reciprocal differentiation and tissue-specific pathogenesis of Th1, Th2, and Th17 cells in graft-versus-host disease. Blood 114, 3101–3112 (2009). [PubMed: 19602708]

30. Farin HF, Karthaus WR, Kujala P, Rakhshandehroo M, Schwank G, Vries RG, Kalkhoven E, Nieuwenhuis EE, Clevers H, Paneth cell extrusion and release of antimicrobial products is directly controlled by immune cell-derived IFN-gamma. J Exp Med 211, 1393–1405 (2014). [PubMed: 24980747]

31. Raetz M, Hwang SH, Wilhelm CL, Kirkland D, Benson A, Sturge CR, Mirpuri J, Vaishnava S, Hou B, Defranco AL, Gilpin CJ, Hooper LV, Yarovinsky F, Parasite-induced TH1 cells and intestinal

dysbiosis cooperate in IFN-gamma-dependent elimination of Paneth cells. Nat Immunol 14, 136–142 (2013). [PubMed: 23263554]

32. Gunther C, Martini E, Wittkopf N, Amann K, Weigmann B, Neumann H, Waldner MJ, Hedrick SM, Tenzer S, Neurath MF, Becker C, Caspase-8 regulates TNF-alpha-induced epithelial necroptosis and terminal ileitis. Nature 477, 335–339 (2011). [PubMed: 21921917]
33. Nava P, Koch S, Laukoetter MG, Lee WY, Kolegraff K, Capaldo CT, Beeman N, Addis C, Gerner-Smidt K, Neumaier I, Skerra A, Li L, Parkos CA, Nusrat A, Interferon-gamma regulates intestinal epithelial homeostasis through converging beta-catenin signaling pathways. Immunity 32, 392–402 (2010). [PubMed: 20303298]
34. Kim JM, Rasmussen JP, Rudensky AY, Regulatory T cells prevent catastrophic autoimmunity throughout the lifespan of mice. Nat Immunol 8, 191–197 (2007). [PubMed: 17136045]
35. Bennett CL, Christie J, Ramsdell F, Brunkow ME, Ferguson PJ, Whitesell L, Kelly TE, Saulsbury FT, Chance PF, Ochs HD, The immune dysregulation, polyendocrinopathy, enteropathy, X-linked syndrome (IPEX) is caused by mutations of FOXP3. Nat Genet 27, 20–21 (2001). [PubMed: 11137993]
36. Chinen T, Volchkov PY, Chervonsky AV, Rudensky AY, A critical role for regulatory T cell-mediated control of inflammation in the absence of commensal microbiota. J Exp Med 207, 2323–2330 (2010). [PubMed: 20921284]
37. Sato T, Vries RG, Snippert HJ, van de Wetering M, Barker N, Stange DE, van Es JH, Abo A, Kujala P, Peters PJ, Clevers H, Single Lgr5 stem cells build crypt-villus structures in vitro without a mesenchymal niche. Nature 459, 262–265 (2009). [PubMed: 19329995]
38. Schuijers J, van der Flier LG, van Es J, Clevers H, Robust cre-mediated recombination in small intestinal stem cells utilizing the olfm4 locus. Stem Cell Reports 3, 234–241 (2014). [PubMed: 25254337]
39. Fu YY, Egorova A, Sobieski C, Kuttiyara J, Calafiore M, Takashima S, Clevers H, Hanash AM, T Cell Recruitment to the Intestinal Stem Cell Compartment Drives Immune-Mediated Intestinal Damage after Allogeneic Transplantation. Immunity 51, 90–103 e103 (2019). [PubMed: 31278057]
40. Abraham C, Dulai PS, Vermeire S, Sandborn WJ, Lessons Learned From Trials Targeting Cytokine Pathways in Patients With Inflammatory Bowel Diseases. Gastroenterology 152, 374–388 e374 (2017). [PubMed: 27780712]
41. Jenq RR, van den Brink MR, Allogeneic haematopoietic stem cell transplantation: individualized stem cell and immune therapy of cancer. Nat Rev Cancer 10, 213–221 (2010). [PubMed: 20168320]
42. Spoerl S, Mathew NR, Bscheider M, Schmitt-Graeff A, Chen S, Mueller T, Verbeek M, Fischer J, Otten V, Schmickl M, Maas-Bauer K, Finke J, Peschel C, Duyster J, Poeck H, Zeiser R, von Bubnoff N, Activity of therapeutic JAK 1/2 blockade in graft-versus-host disease. Blood 123, 3832–3842 (2014). [PubMed: 24711661]
43. Abedin S, McKenna E, Chhabra S, Pasquini M, Shah NN, Jerkins J, Baim A, Runaas L, Longo W, Drobyski W, Hari PN, Hamadani M, Efficacy, Toxicity, and Infectious Complications in Ruxolitinib-Treated Patients with Corticosteroid-Refractory Graft-versus-Host Disease after Hematopoietic Cell Transplantation. Biol Blood Marrow Transplant, (2019).
44. von Bubnoff N, Ihorst G, Grishina O, Rothling N, Bertz H, Duyster J, Finke J, Zeiser R, Ruxolitinib in GvHD (RIG) study: a multicenter, randomized phase 2 trial to determine the response rate of Ruxolitinib and best available treatment (BAT) versus BAT in steroid-refractory acute graft-versus-host disease (aGvHD) (NCT02396628). BMC Cancer 18, 1132 (2018). [PubMed: 30453910]
45. Zeiser R, Burchert A, Lengerke C, Verbeek M, Maas-Bauer K, Metzelder SK, Spoerl S, Ditschkowski M, Ecsedi M, Sockel K, Ayuk F, Ajib S, de Fontbrune FS, Na IK, Penter L, Holtick U, Wolf D, Schuler E, Meyer E, Apostolova P, Bertz H, Marks R, Lubbert M, Wasch R, Scheid C, Stolzel F, Ordemann R, Bug G, Kobbe G, Negrin R, Brune M, Spyridonidis A, Schmitt-Graff A, van der Velden W, Huls G, Mielke S, Grigoleit GU, Kuball J, Flynn R, Ihorst G, Du J, Blazar BR, Arnold R, Kroger N, Passweg J, Halter J, Socie G, Beelen D, Peschel C, Neubauer A, Finke J, Duyster J, von Bubnoff N, Ruxolitinib in corticosteroid-refractory graft-versus-host disease after

allogeneic stem cell transplantation: a multicenter survey. Leukemia 29, 2062–2068 (2015). [PubMed: 26228813]

46. Yin X, Farin HF, van Es JH, Clevers H, Langer R, Karp JM, Niche-independent high-purity cultures of Lgr5+ intestinal stem cells and their progeny. Nat Methods 11, 106–112 (2014). [PubMed: 24292484]
47. Ni X, Song Q, Cassady K, Deng R, Jin H, Zhang M, Dong H, Forman S, Martin PJ, Chen YZ, Wang J, Zeng D, PD-L1 interacts with CD80 to regulate graft-versus-leukemia activity of donor CD8+ T cells. J Clin Invest 127, 1960–1977 (2017). [PubMed: 28414296]
48. Teshima T, Ordemann R, Reddy P, Gagin S, Liu C, Cooke KR, Ferrara JL, Acute graft-versus-host disease does not require alloantigen expression on host epithelium. Nat Med 8, 575–581 (2002). [PubMed: 12042807]
49. Koyama M, Kuns RD, Olver SD, Raffelt NC, Wilson YA, Don AL, Lineburg KE, Cheong M, Robb RJ, Markey KA, Varelias A, Malissen B, Hammerling GJ, Clouston AD, Engwerda CR, Bhat P, MacDonald KP, Hill GR, Recipient nonhematopoietic antigen-presenting cells are sufficient to induce lethal acute graft-versus-host disease. Nat Med 18, 135–142 (2011). [PubMed: 22127134]
50. Agudo J, Park ES, Rose SA, Alibo E, Sweeney R, Dhainaut M, Kobayashi KS, Sachidanandam R, Baccarini A, Merad M, Brown BD, Quiescent Tissue Stem Cells Evade Immune Surveillance. Immunity 48, 271–285 e275 (2018). [PubMed: 29466757]
51. Biton M, Haber AL, Rogel N, Burgin G, Beyaz S, Schnell A, Ashenberg O, Su CW, Smillie C, Shekhar K, Chen Z, Wu C, Ordovas-Montanes J, Alvarez D, Herbst RH, Zhang M, Tirosh I, Dionne D, Nguyen LT, Xifaras ME, Shalek AK, von Andrian UH, Graham DB, Rozenblatt-Rosen O, Shi HN, Kuchroo V, Yilmaz OH, Regev A, Xavier RJ, T Helper Cell Cytokines Modulate Intestinal Stem Cell Renewal and Differentiation. Cell 175, 1307–1320 e1322 (2018). [PubMed: 30392957]
52. Nava P, Kamekura R, Quiros M, Medina-Contreras O, Hamilton RW, Kolegraff KN, Koch S, Candelario A, Romo-Parra H, Laur O, Hilgarth RS, Denning TL, Parkos CA, Nusrat A, IFNgamma-induced suppression of beta-catenin signaling: evidence for roles of Akt and 14.3.3zeta. Mol Biol Cell 25, 2894–2904 (2014). [PubMed: 25079689]
53. Capaldo CT, Beeman N, Hilgarth RS, Nava P, Louis NA, Naschberger E, Sturzl M, Parkos CA, Nusrat A, IFN-gamma and TNF-alpha-induced GBP-1 inhibits epithelial cell proliferation through suppression of beta-catenin/TCF signaling. Mucosal Immunol 5, 681–690 (2012). [PubMed: 22692453]
54. Shoshkes-Carmel M, Wang YJ, Wangensteen KJ, Toth B, Kondo A, Massasa EE, Itzkovitz S, Kaestner KH, Subepithelial telocytes are an important source of Wnts that supports intestinal crypts. Nature 557, 242–246 (2018). [PubMed: 29720649]
55. Kabiri Z, Greicius G, Madan B, Biechele S, Zhong Z, Zaribafzadeh H, Edison, Aliyev J, Wu Y, Bunte R, Williams BO, Rossant J, Virshup DM, Stroma provides an intestinal stem cell niche in the absence of epithelial Wnts. Development 141, 2206–2215 (2014). [PubMed: 24821987]
56. Jadhav U, Saxena M, O'Neill NK, Saadatpour A, Yuan GC, Herbert Z, Murata K, Shivdasani RA, Dynamic Reorganization of Chromatin Accessibility Signatures during Dedifferentiation of Secretory Precursors into Lgr5+ Intestinal Stem Cells. Cell Stem Cell 21, 65–77 e65 (2017). [PubMed: 28648363]
57. Tetteh PW, Basak O, Farin HF, Wiebrands K, Kretzschmar K, Begthel H, van den Born M, Korving J, de Sauvage F, van Es JH, van Oudenaarden A, Clevers H, Replacement of Lost Lgr5-Positive Stem Cells through Plasticity of Their Enterocyte-Lineage Daughters. Cell Stem Cell 18, 203–213 (2016). [PubMed: 26831517]
58. Buczacki SJ, Zecchini HI, Nicholson AM, Russell R, Vermeulen L, Kemp R, Winton DJ, Intestinal label-retaining cells are secretory precursors expressing Lgr5. Nature 495, 65–69 (2013). [PubMed: 23446353]
59. van Es JH, Sato T, van de Wetering M, Lyubimova A, Nee AN, Gregorieff A, Sasaki N, Zeinstra L, van den Born M, Korving J, Martens AC, Barker N, van Oudenaarden A, Clevers H, Dll1+ secretory progenitor cells revert to stem cells upon crypt damage. Nat Cell Biol 14, 1099–1104 (2012). [PubMed: 23000963]
60. Chen HC, Kanai M, Inoue-Yamauchi A, Tu HC, Huang Y, Ren D, Kim H, Takeda S, Reyna DE, Chan PM, Ganesan YT, Liao CP, Gavathiotis E, Hsieh JJ, Cheng EH, An interconnected

hierarchical model of cell death regulation by the BCL-2 family. Nat Cell Biol 17, 1270–1281 (2015). [PubMed: 26344567]

61. Czabotar PE, Lessene G, Strasser A, Adams JM, Control of apoptosis by the BCL-2 protein family: implications for physiology and therapy. Nat Rev Mol Cell Biol 15, 49–63 (2014). [PubMed: 24355989]
62. Platanias LC, Mechanisms of type-I- and type-II-interferon-mediated signalling. Nat Rev Immunol 5, 375–386 (2005). [PubMed: 15864272]
63. Kleppe M, Spitzer MH, Li S, Hill CE, Dong L, Papalexi E, De Groote S, Bowman RL, Keller M, Koppikar P, Rapaport FT, Teruya-Feldstein J, Gandara J, Mason CE, Nolan GP, Levine RL, Jak1 Integrates Cytokine Sensing to Regulate Hematopoietic Stem Cell Function and Stress Hematopoiesis. Cell Stem Cell 21, 489–501 e487 (2017). [PubMed: 28965767]
64. Rothenberg ME, Nusse Y, Kalisky T, Lee JJ, Dalerba P, Scheeren F, Lobo N, Kulkarni S, Sim S, Qian D, Beachy PA, Pasricha PJ, Quake SR, Clarke MF, Identification of a cKit(+) colonic crypt base secretory cell that supports Lgr5(+) stem cells in mice. Gastroenterology 142, 1195–1205 e1196 (2012). [PubMed: 22333952]
65. Shroyer NF, Helmrath MA, Wang VY, Antalffy B, Henning SJ, Zoghbi HY, Intestine-specific ablation of mouse atonal homolog 1 (Math1) reveals a role in cellular homeostasis. Gastroenterology 132, 2478–2488 (2007). [PubMed: 17570220]
66. Alpdogan O, Muriglan SJ, Eng JM, Willis LM, Greenberg AS, Kappel BJ, van den Brink MR, IL-7 enhances peripheral T cell reconstitution after allogeneic hematopoietic stem cell transplantation. J Clin Invest 112, 1095–1107 (2003). [PubMed: 14523046]
67. Yarilin D, Xu K, Turkekul M, Fan N, Romin Y, Fijisawa S, Barlas A, Manova-Todorova K, Machine-based method for multiplex in situ molecular characterization of tissues by immunofluorescence detection. Sci Rep 5, 9534 (2015). [PubMed: 25826597]
68. Fu YY, Lin CW, Enikolopov G, Sibley E, Chiang AS, Tang SC, Microtome-free 3-dimensional confocal imaging method for visualization of mouse intestine with subcellular-level resolution. Gastroenterology 137, 453–465 (2009). [PubMed: 19447107]
69. Fu YY, Peng SJ, Lin HY, Pasricha PJ, Tang SC, 3-D imaging and illustration of mouse intestinal neurovascular complex. Am J Physiol Gastrointest Liver Physiol 304, G1–11 (2013). [PubMed: 23086917]
70. Merlos-Suarez A, Barriga FM, Jung P, Iglesias M, Cespedes MV, Rossell D, Sevillano M, Hernando-Momblona X, da Silva-Diz V, Munoz P, Clevers H, Sancho E, Mangues R, Batlle E, The intestinal stem cell signature identifies colorectal cancer stem cells and predicts disease relapse. Cell Stem Cell 8, 511–524 (2011). [PubMed: 21419747]
71. Cooke KR, Kobzik L, Martin TR, Brewer J, Delmonte J Jr., Crawford JM, Ferrara JL, An experimental model of idiopathic pneumonia syndrome after bone marrow transplantation: I. The roles of minor H antigens and endotoxin. Blood 88, 3230–3239 (1996). [PubMed: 8963063]
72. Schewe M, Franken PF, Sacchetti A, Schmitt M, Joosten R, Bottcher R, van Royen ME, Jeammet L, Payre C, Scott PM, Webb NR, Gelb M, Cormier RT, Lambeau G, Fodde R, Secreted Phospholipases A2 Are Intestinal Stem Cell Niche Factors with Distinct Roles in Homeostasis, Inflammation, and Cancer. Cell Stem Cell 19, 38–51 (2016). [PubMed: 27292189]
73. Dobin A, Davis CA, Schlesinger F, Drenkow J, Zaleski C, Jha S, Batut P, Chaisson M, Gingeras TR, STAR: ultrafast universal RNA-seq aligner. Bioinformatics 29, 15–21 (2013). [PubMed: 23104886]
74. Engstrom PG, Steijger T, Sipos B, Grant GR, Kahles A, Ratsch G, Goldman N, Hubbard TJ, Harrow J, Guigo R, Bertone P, R. Consortium, Systematic evaluation of spliced alignment programs for RNA-seq data. Nat Methods 10, 1185–1191 (2013). [PubMed: 24185836]

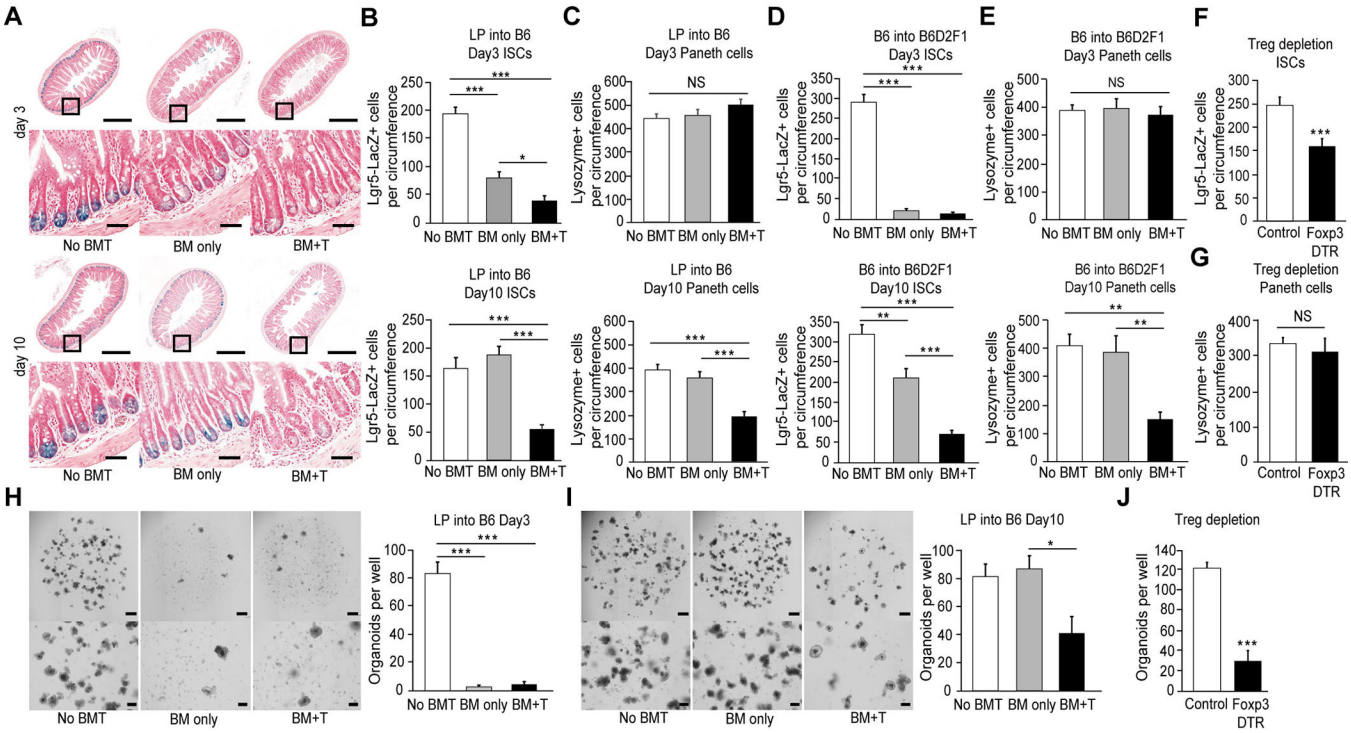

Fig. 1. Alloreactive and autoreactive immune responses injure the intestinal stem cell compartment.

(**A** to **C**) LP-into-Lgr5-LacZ-B6 MHC-matched BMT. (**A**) Representative images of SI (ileum) Lgr5-LacZ staining on day 3 and day 10 post-BMT. Scale bars = 500μm (Upper) or 50μm (Lower). (**B**) SI ISC frequency (n = 8–25 independent sections/group) and (**C**) SI lysozyme^{+} Paneth cell frequency (n = 6–15 independent sections/group) on day 3 and day 10 post-BMT (**D** and **E**) B6-into-Lgr5-LacZ-BDF1 MHC-mismatched BMT, SI ISC frequency (**D**, n = 5–15 independent sections/group) and SI lysozyme^{+} Paneth cell frequency (**E**, n = 6–13 independent sections/group) on day 3 and day 10 post-BMT. (**F** and **G**) Foxp3-WT and Foxp3-DTR mice treated with DT. SI ISC frequency (**F**) and SI lysozyme^{+} Paneth cell frequency (**G**) 5 days after DT treatment (n = 19–20 independent sections/group). (**H** and **I**) Representative images and numbers of day 5 SI organoids from recipients day 3 (**H**) and day 10 (**I**) after LP-into-B6 BMT. Organoid culture from 150 crypts. Scale bars = 500μm (Upper) or 200μm (Lower). (n = 3 mice/group). (**J**) Day 5 SI organoid numbers from 150 crypts harvested 9 days after DT treatment (n = 4 mice/group). Data are mean and s.e.m.; comparisons performed with t-tests (two groups) or one-way ANOVA (multiple groups); *P < 0.05, **P < 0.01, ***P < 0.001. Data are representative of at least two independent experiments, or combined from two experiments (A to E)

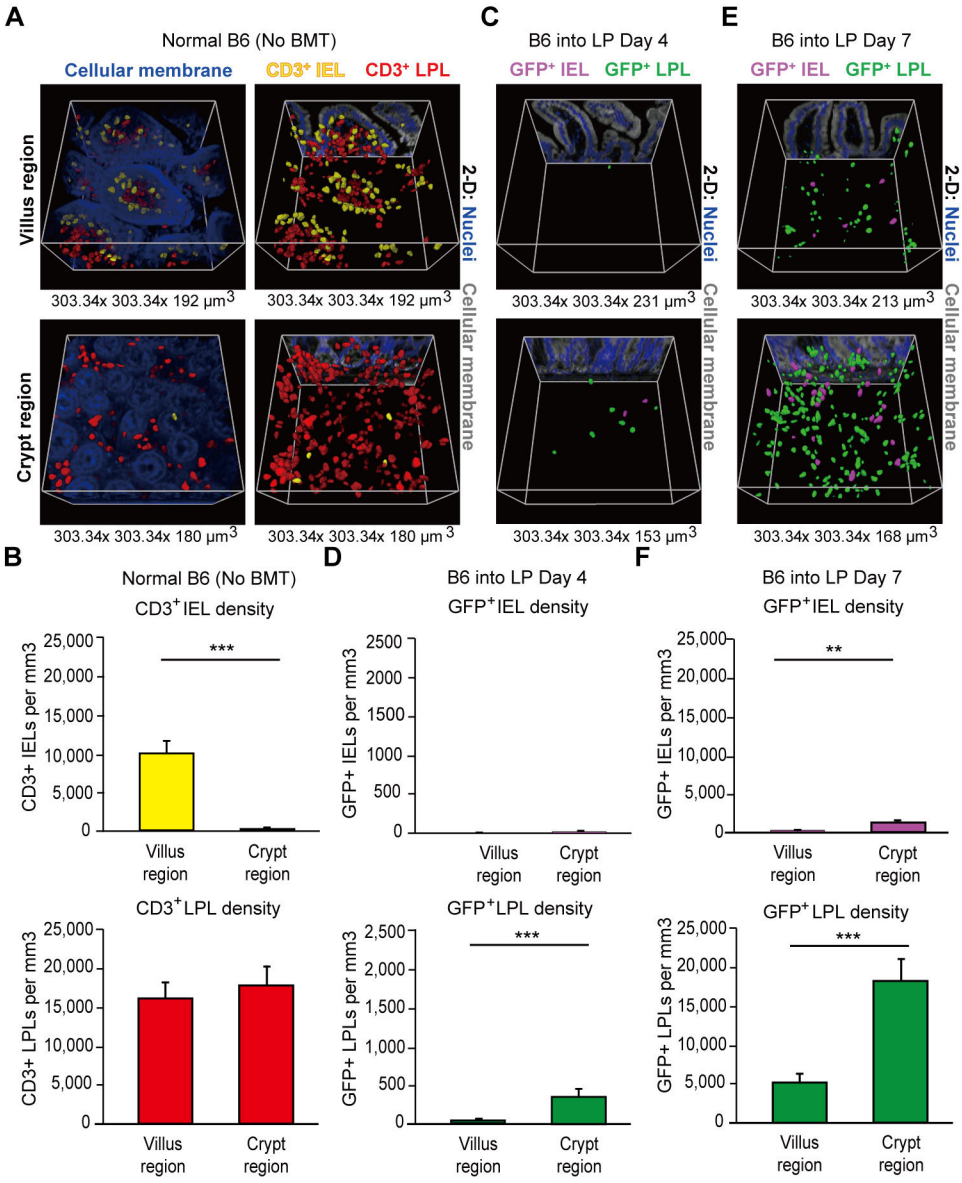

Fig. 2. Donor T cells infiltrate the epithelial layer and lamina propria in the crypt region after bone marrow transplantation.

3-D whole-mount immunofluorescent confocal imaging of mouse ileum. (**A** and **B**) T cells in normal B6 mice were identified by anti-CD3 immunofluorescence. (**A**) Left panels: Representative 3-D projection images of full-thickness SI tissue divided into villus and crypt regions, with cellular membrane staining (DiD lipophilic dye; blue) indicating the tissue architecture utilized for distinguishing IELs and LPLs within the ileum; yellow, $CD3^+$ IELs; red, $CD3^+$ LPLs. Right panels: 3-D projections of $CD3^+$ IELs and $CD3^+$ LPLs in the villus and crypt regions, with cellular membrane staining removed and tissue orientation (and thus T cell localization within the 3-D tissues) indicated by 2-D slices shown on the posterior projection walls. (**B**) Quantification of $CD3^+$ IEL and $CD3^+$ LPL densities in normal B6 (n = 6 independent 3-D views/group). (**C** to **F**) B6-into-LP allogeneic BMT was performed using wild-type B6 marrow and purified GFP^+ B6 T cells, with donor T cells in the

epithelium shown in purple and donor T cells in the lamina propria shown in green. (**C**) Representative 3-D projections and (**D**) quantifications of donor T cells in the villus and crypt regions 4 days post-BMT (n = 24 independent 3-D views/group combined from 2 transplants). (**E**) Representative 3-D projections and (**F**) quantifications of donor T cells in the villus and crypt regions 7 days post-BMT (n = 12 independent 3-D views/group). Tissue orientation and T cell localization are again indicated by 2-D slices shown on the posterior walls of the 3-D projections. Graphs indicate mean and s.e.m.; comparisons performed with t-tests; **P < 0.01, ***P < 0.001. Data are representative of two independent experiments unless otherwise mentioned.

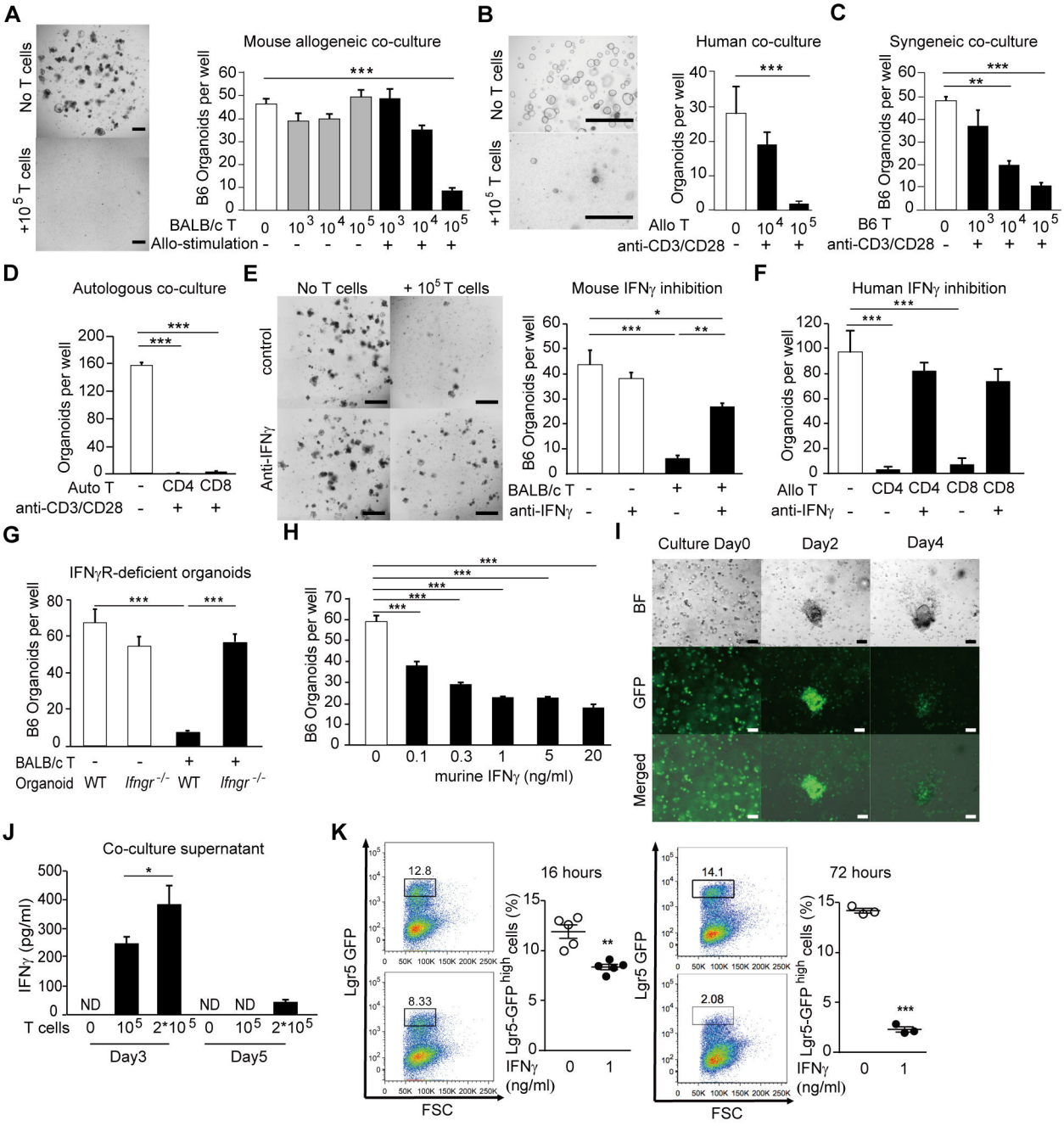

Fig. 3. T-cell-derived IFNγ targets intestinal epithelium leading to reduction of Lgr5$^+$ stem cells.

(**A**) Representative images and number of SI organoids after co-culture of B6 organoid cells with activated by allogeneic B6 dendritic cells or naive allogeneic BALB/c T cells (culture day 7, n = 3–6 wells/group); scale bars = 500μm. (**B**) Representative images and number of human SI organoids cultured with human allogeneic CD8$^+$ T cells (culture day 7, n = 7–13 wells/group); scale bars = 1000μm. (**C**) Numbers of B6 SI organoids after culture with anti-CD3/CD28-activated B6 syngeneic T cells (culture day 7, n = 3 wells/group). (**D**) Human LI organoids after culture with autologous human CD4$^+$ and CD8$^+$ T cells (culture day 7, n = 3 wells/group). (**E**) Representative images and numbers of B6 SI organoids after culture with

anti-CD3/CD28-activated BALB/c T cells and anti-IFNγ neutralizing antibodies (culture day 7, n = 4 wells/group); scale bars = 500μm. (**F**) Human SI organoids after culture with human allogeneic T cells and anti-IFNγ (culture day 7, n = 9 wells/group). (**G**) WT or *Ifngr*$^{-/-}$ B6 SI organoids cultured with BALB/c T cells (culture day 7, n = 4 wells/group). (**H**) B6 SI organoids after culture with rmIFNγ (culture day 7, n = 3 wells/group). (**I**) Representative images after co-culture of BDF1 organoid cells with GFP^{+} allogeneic B6 T cells. Shown are bright field (upper), fluorescent (middle), or overlap (lower) images; scale bars = 50μm. (**J**) IFNγ ELISA on supernatants from culture of B6 SI organoids with BALB/c T cells (n = 4–8 wells/group; ND, not detected. (**K**) FACS analysis of Lgr5-GFP^{high} ISCs in organoids cultured with rmIFNγ for 16 or 72 hours (n = 3–5 wells/group). Data are mean and s.e.m.; comparisons performed with t-tests (two groups) or one-way ANOVA (multiple groups); *P < 0.05, **P < 0.01, ***P < 0.001. Data are representative of at least two independent experiments, or combined from two or three (B, F, J) independent experiments.

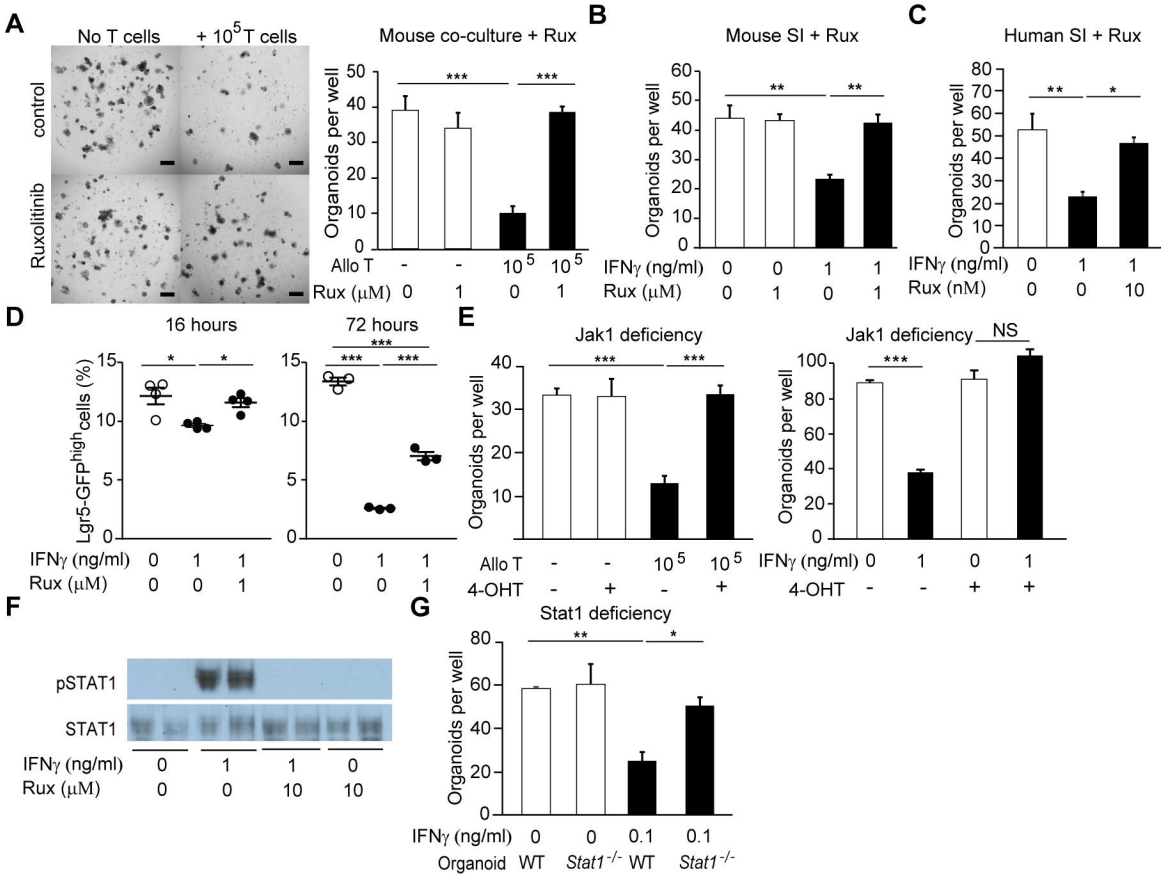

Fig. 4. JAK/STAT inhibition protects intestinal stem cells from IFNγ.

(**A**) Representative images and numbers of B6 organoids after culture with BALB/c T cells and ruxolitinib (culture day 7, n = 4 wells/group); scale bars = 500μm. (**B**) Numbers of B6 SI organoid cells after culture with rmIFNγ and ruxolitinib (culture day 7, n = 4 wells/group). (**C**) Human SI organoids cultured with rhIFNγ (culture day 7, n = 3 wells/group) and ruxolitinib. (**D**) FACS analysis of Lgr5–GFP^{high} ISCs in organoids cultured with rmIFNγ and ruxolitinib for 16 or 72 hours (n = 3–4 wells/group). (**E**) Jak1-deficient B6 SI organoids from *Jak1*$^{fl/fl}$xRosa-cre-ert2 mice cultured with BALB/c T cells or rmIFNγ (culture day 7, n = 4 wells/group). (**F**) Crypt pSTAT1 western blots after 30 minutes incubation with rmIFNγ +/− ruxolitinib. (**G**) WT or *Stat1*$^{-/-}$ B6 SI organoids cultured with rmIFNγ (culture day 7, n = 4 wells/group). Graphs indicate mean and s.e.m.; t-tests (two groups) or one-way ANOVA (multiple groups); *P < 0.05, **P < 0.01, ***P < 0.001. Data are representative of at least two independent experiments.

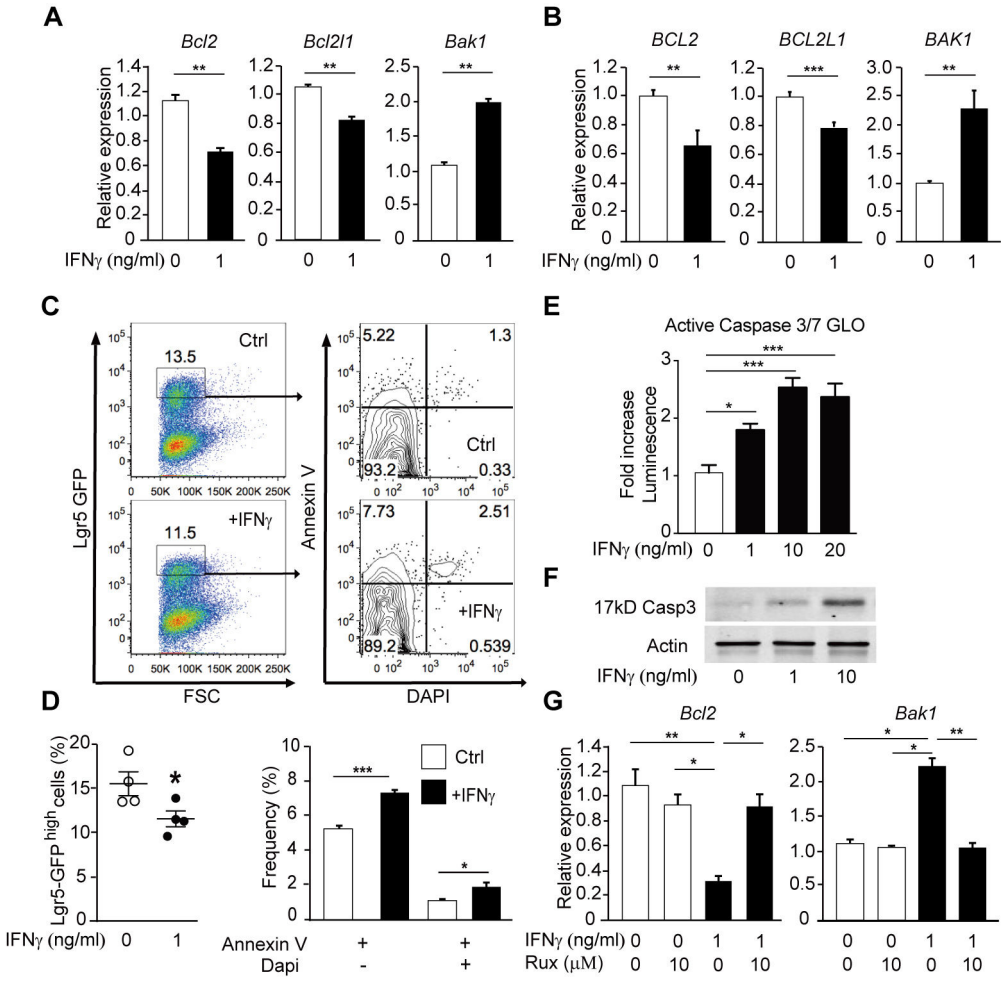

Fig. 5. IFNγ programs stem cell death.

(**A**) Apoptosis-related genes expression in mouse SI organoids cultured with rmIFNγ for 6 hours (n = 6 wells/group); Mann–Whitney U analysis. (**B**) Apoptosis-related genes expression in human SI organoids cultured with rhIFNγ for 24 hours (n = 9–10 wells/group, data are from 3 different SI donors); Mann–Whitney U analysis. (**C** and **D**) FACS plots (**C**) and quantifications (**D**) of Lgr5-GFP^{high} cells and Annexin V analysis from SI organoids cultured with rmIFNγ for 16 hours (n = 4 wells/group). (**E**) Relative caspase-3/7 activity as evaluated by Caspase-Glo assay; fold increase over baseline after treatment with rhIFNγ for 24 hours (n = 6 wells/group). (**F**) Human organoid cleaved caspase-3 western blot after 48 hours incubation with rhIFNγ. (**G**) Apoptosis-related genes expression in mouse SI organoids cultured with rmIFNγ and ruxolitinib for 24 hours (n = 6 wells/group); Kruskal–Wallis analysis. Graphs indicate mean and s.e.m.; comparisons performed with t-tests (two groups) or one-way ANOVA (multiple groups) unless otherwise stated; *P < 0.05, **P < 0.01, ***P < 0.001. Data are representative of two, or combined from two (E) independent experiments.

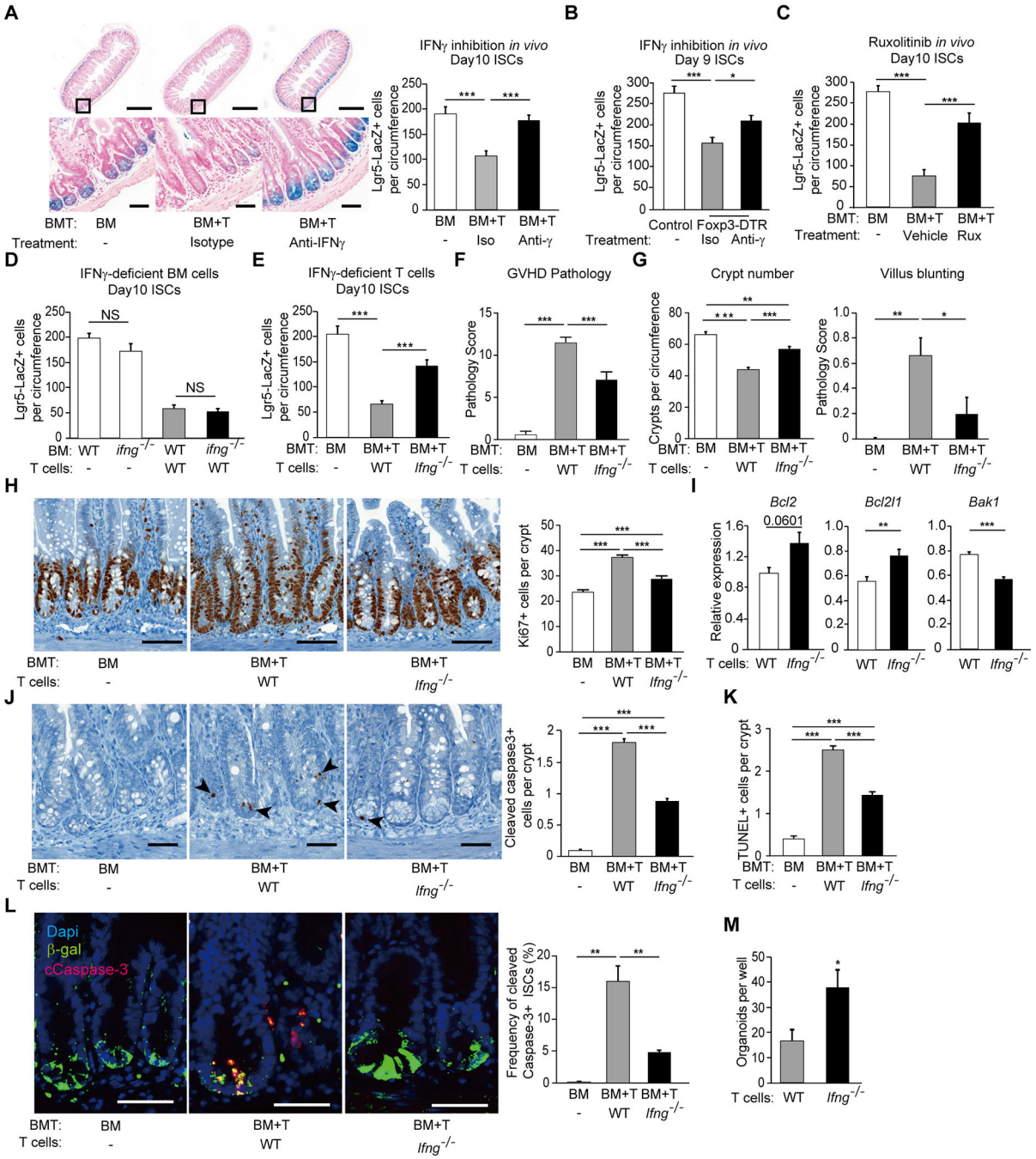

Fig. 6. T-cell-derived-IFNγ decreases ISCs *in vivo*.

(**A**) ISCs 10 days after LP-into-B6 BMT with isotype or anti-IFNγ antibodies. Representative images and frequency of SI Lgr5-LacZ^{+} ISCs (n = 15–27 independent sections/group); scale bars = 500μm (Upper) or 50μm (Lower). (**B**) SI Lgr5^{+} ISCs in Foxp3-DTR^{+} or Foxp3-DTR^{-} Lgr5-LacZ reporter mice 5 days after DT treatment along with Isotype or anti-IFNγ antibodies (n = 29–31 independent sections/group). (**C**) Frequency of SI Lgr5-LacZ^{+} ISCs 10 days after LP-into-B6 BMT with vehicle or ruxolitinib (n = 6–10 independent sections/group). (**D**) Frequency of SI Lgr5-LacZ^{+} ISCs 10 days after B6-into-

BDF1 BMT with wild type or *Ifng*$^{-/-}$ marrow (n = 5–13 independent sections/group). (**E** to **M**) B6-into-BDF1 BMT with wild type or *Ifng*$^{-/-}$ T cells. (**E**) Frequency of SI Lgr5-LacZ^{+} ISCs (n = 5–11 independent sections/group). (**F**) Intestinal GVHD histopathology score 10 days after BMT (n = 6–12 mice). (**G**) Crypt numbers (n = 6–21 independent sections/group) and villus blunting histopathology scores (n = 6–12 mice/group) 10 days after BMT. (**H**) Representative images and quantification of Ki67 IHC in the crypt area 10 days after BMT (n = 47–77 crypts/group); scale bars = 100μm. (**I**) Apoptosis-related genes expression in mouse SI crypts 10 days after BMT (n = 10 mice; Mann–Whitney U analysis). (**J**) Images and quantification of crypt cleaved caspase-3 IHC 10 days after BMT. Arrows indicate cleaved caspase-3^{+} apoptotic crypt cells (n = 489–974 crypts/group); scale bars = 50μm. (**K**) Quantification of crypt TUNEL staining 10 days after BMT (n = 251–491 crypts/group). (**L**) Double immunofluorescent staining of β-gal (green) and cleaved caspase-3 (red) from Lgr5-LacZ recipient mice 10 days after BMT. Shown are representative images and average frequencies of cleaved caspase-3^{+} apoptotic ISCs per mouse ileum as a percentage of the total Lgr5^{+} ISCs detected; scale bars = 50μm. (**M**) Day 5 SI organoid numbers per 100 crypts cultured 10 days after BMT (n = 5–7 mice/group). Graphs demonstrate mean and s.e.m.; comparisons performed with t-tests (two groups) or one-way ANOVA (multiple groups) unless otherwise stated; *P<0.05, **P<0.01, ***P<0.001. Data are representative of two, or combined from two (A, B, F, G and I) independent experiments.

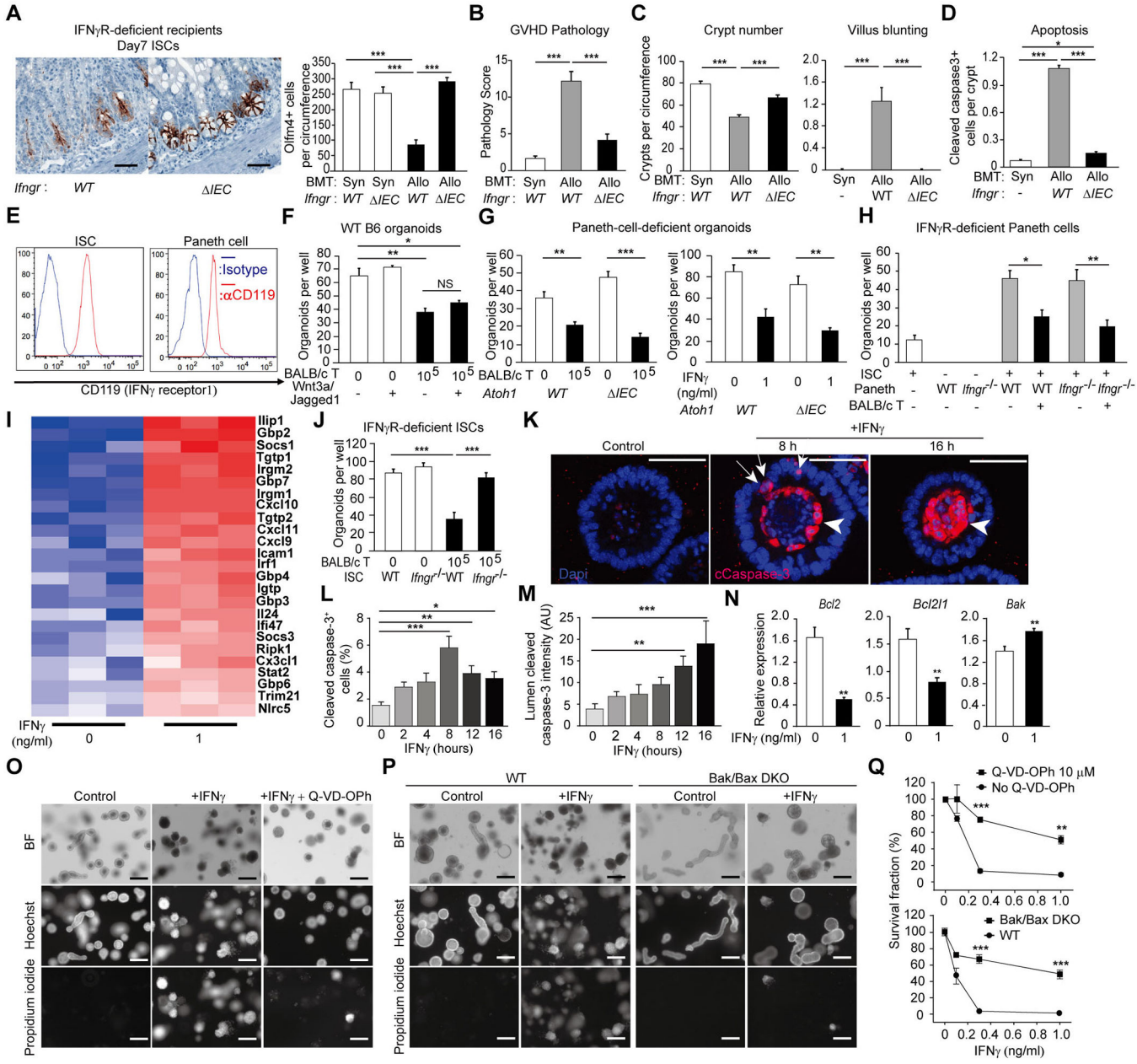

Fig. 7. IFNγ directly targets intestinal stem cells and induces apoptosis.

(**A** to **D**) Allogeneic B10.Br-into-B6 (Allo) or syngeneic B6-into-B6 (Syn) BMT using *Ifngr*$^{fl/fl}$xVillin-Cre (*Ifngr*$^{\Delta IEC}$) or Cre-negative *Ifngr*$^{fl/fl}$ (*Ifngr*^{WT}) littermate controls. (**A**) Representative images and frequency of SI (ileum) IHC for Olfm4^{+} ISCs 7 days after BMT (n = 6–17 independent sections/group); scale bars = 100μm. (**B**) Intestinal GVHD histopathology score 9 days after BMT (n = 3–5 mice/group). (**C**) Crypt number quantification (n = 9–17 independent sections/group) and villus blunting histopathologic scoring 9 days after BMT (n = 3–5 mice/group). (**D**) Quantification of crypt cleaved caspase-3 (cCaspase-3) IHC 9 days after BMT (n = 489–974 crypts/group). (**E**) FACS analysis of CD119 (IFNγR1) expression on ISCs and Paneth cells. (**F**) Numbers of B6 SI

organoids 7 days after culture with BALB/c T cells +/− Wnt3a and Jagged1 (n = 3 wells/group). (**G**) Paneth-cell-deficient *Atoh1*$^{\Delta IEC}$ SI organoids cultured in WNT3-supplemented ENR media for 7 days +/− BALB/c T cells or IFNγ (n = 4 wells/group). (**H**) SI organoids from sort-purified SI Lgr5-GFP^{high} ISCs and sort-purified Paneth cells cultured for 7 days +/− BALB/c T cells (n = 3–6 wells/group). (**I**) RNAseq indicating IFNγ-responsive gene expression in sorted Lgr5-GFP^{high} ISCs incubated with IFNγ for 1.5 hours. (**J**) Organoids from sorted WT or *Ifngr*$^{-/-}$ Lgr5-GFP^{high} SI ISCs cultured for 6 days +/− BALB/c T cells (n = 7–8 wells/group). (**K** to **Q**) ISC colonies cultured in WENR with HDAC and GSK3β inhibition +/− IFNγ. (**K**) Representative confocal images of cleaved caspase-3 (cCaspase-3) immunofluorescence in ISC colonies cultured +/− IFNγ (culture day 6, arrows indicate apoptotic ISCs in the cellular layer, and arrow heads indicate apoptotic ISCs in the colony lumen), scale bars = 50μm. (**L**) Frequency of epithelial-layer cCaspase-3^{+} ISCs (n = 40–72 colonies/group). (**M**) cCaspase-3 staining intensity in the lumen area (n = 76–136 colonies/group). (**N**) qPCR analysis of apoptosis-related genes in mouse SI ISC colonies cultured with rmIFNγ for 24 hours (n = 6 wells/group; Mann–Whitney U analysis). (**O** to **Q**) Representative images and viability quantification of ISC colonies cultured with IFNγ. Images show bright field microscopy (Upper), Hoechst staining (Middle), or propidium iodide (Lower); scale bars = 200 μm. (**O**) Images of Lgr5-GFP^{+} SI ISC colonies cultured with rmIFNγ +/− caspase inhibitor Q-VD-OPh (culture day 7). (**P**) Images of SI ISC colonies initiated from sorted WT or Bak/Bax double knockout (DKO) SI ISCs cultured with IFNγ (culture day 7). (**Q**) Quantification of ISC colony survival after cultured with IFNγ (n = 3 colonies/group); t-tests at each concentration of IFNγ. Graphs indicate mean and s.e.m.; comparisons performed with one-way ANOVA unless otherwise stated; *P<0.05, **P<0.01, ***P<0.001. Data are representative of at least two, or combined from three independent experiments (I).